

Coherence Time Extension by Large Scale Optical Spin Polarization in a Rare-Earth Doped Crystal

Sacha Welinski,^{1,*} Alexey Tiranov,^{2,†} Moritz Businger,² Alban Ferrier,^{1,3} Mikael Afzelius,² and Philippe Goldner^{1,‡}

¹*Chimie ParisTech, PSL University, CNRS, Institut de Recherche de Chimie Paris, 75005 Paris, France*

²*Département de Physique Appliquée, Université de Genève, CH-1211 Genève, Switzerland*

³*Sorbonne Universités, Faculté des Sciences et Ingénierie, UFR 933, 75005 Paris, France*

(Dated: October 18, 2019)

Optically addressable spins are actively investigated in quantum communication, processing and sensing. Optical and spin coherence lifetimes, which determine quantum operation fidelity and storage time, are often limited by spin-spin interactions, which can be decreased by polarizing spins in their lower energy state using large magnetic fields and/or mK range temperatures. Here, we show that optical pumping of a small fraction of ions with a fixed frequency laser, coupled with spin-spin interactions and spin diffusion, leads to substantial spin polarization in a paramagnetic rare earth doped crystal, $^{171}\text{Yb}^{3+}:\text{Y}_2\text{SiO}_5$. Indeed, up to more than 90 % spin polarizations have been achieved at 2 K and zero magnetic field. Using this spin polarization mechanism, we furthermore demonstrate an increase in optical coherence lifetime from 0.3 ms to 0.8 ms, due to a strong decrease in spin-spin interactions. This effect opens the way to new schemes for obtaining long optical and spin coherence lifetimes in various solid-state systems such as ensembles of rare earth ions or color centers in diamond, which is of interest for a broad range of quantum technologies.

Systems with both spin and optical transitions offer improved functionalities for quantum technologies¹. They allow storage and entanglement of photonic quantum states for quantum communications^{2,3}, interfacing processing nodes with optical networks for distributed quantum computing⁴ or efficient detection for quantum sensing⁵. Key parameters in these centers are the coherence lifetimes of optical and spin transitions, which affect storage time, operation fidelity and sensitivity. In the solid state, major sources of perturbation to quantum states are due to magnetic fluctuations in the centers environment that couple to transitions through magnetic dipole-dipole interactions. This magnetic noise is often due to flips of electron or nuclear spins carried by the host material atoms⁶, impurities or defects⁷, or the centers of interest themselves^{8,9}. Considerable work has been devoted to engineer these ensembles, known as the spin bath, in order to reduce their detrimental effect on coherence lifetimes. This includes isotope purification to eliminate elements with non-zero spins^{10,11} and application of high magnetic fields^{12,13} and/or very low temperatures¹⁴ to freeze spins in their lower energy state. Another approach is to decouple the optically addressable spins from the bath by using clock transitions that are insensitive to magnetic field fluctuations in first order¹⁵⁻¹⁷ or by filtering out bath fluctuations by dynamical techniques^{18,19}. Although they can be very efficient, these methods may be complex to implement.

Here, we show that optical pumping (OP) of a very small fraction ($\approx 0.5\%$) of spins in an ensemble can lead, through spin diffusion, to a polarization of this ensemble larger than 90 %. Furthermore, this large scale change in spin populations can be tuned to strongly decrease spin-spin interactions and in turn extend optical coherence lifetimes close to the radiative limit. This process, which we call Diffusion Enhanced Optical Pumping (DEOP), is illustrated in Fig. 1a. A narrow laser optically pumps a small subset of spins randomly located in the laser excitation volume (labeled 'optical spins' in Fig. 1a, left). The optical spins exchange energy with neighboring spins through flip-flop processes. The latter are initially in thermal equilibrium ('thermal spins'), but because they interact with the strongly polarized optical spins, they become polarized as well ('polarized spins') as shown in Fig. 1a, center. The spin polarization gradually diffuses over the whole optically excited volume through further flip-flop interactions between polarized and thermal spins (Fig. 1a, right). As shown in this Article, DEOP allows coherence lifetime extension by creating specific, highly out of equilibrium, population distributions among spin levels, a feature difficult to obtain by using magnetic field, low temperature, or by optical pumping alone.

We demonstrate DEOP in a rare earth (RE) doped crystal, $^{171}\text{Yb}^{3+}:\text{Y}_2\text{SiO}_5$ (YSO). These materials, in which optical and spin coherence lifetime can reach up to ms and hours at low temperatures^{6,12,20}, are actively investigated for spin based quantum photonic applications ranging from quantum memories^{2,21-24}, processors²⁵ and single photon sources^{26,27} to optical-microwave transducers^{28,29}. $^{171}\text{Yb}^{3+}:\text{YSO}$, in which long coherence lifetimes have been shown for both optical and spin transitions at zero magnetic field¹⁷, is particularly promising in this area³⁰⁻³³. Using DEOP, we obtained spin polarizations $> 90\%$, a much stronger effect than previously reported in ruby³⁴. Thanks to its spin ensemble tailoring capabilities, we then used DEOP to reduce or enhance specific spin-spin interactions, and in particular extend $^{171}\text{Yb}^{3+}$ optical coherence lifetimes T_2 to about 800 μs , a 2.5-fold increase compared to thermal equilibrium. This is the longest optical T_2 reported for any paramagnetic solid state system at zero or very-low magnetic fields, which can be especially interesting for interfacing with superconducting qubits and resonators. DEOP uses a counter intuitive scheme that exploits interactions to ultimately control them and should be effective in

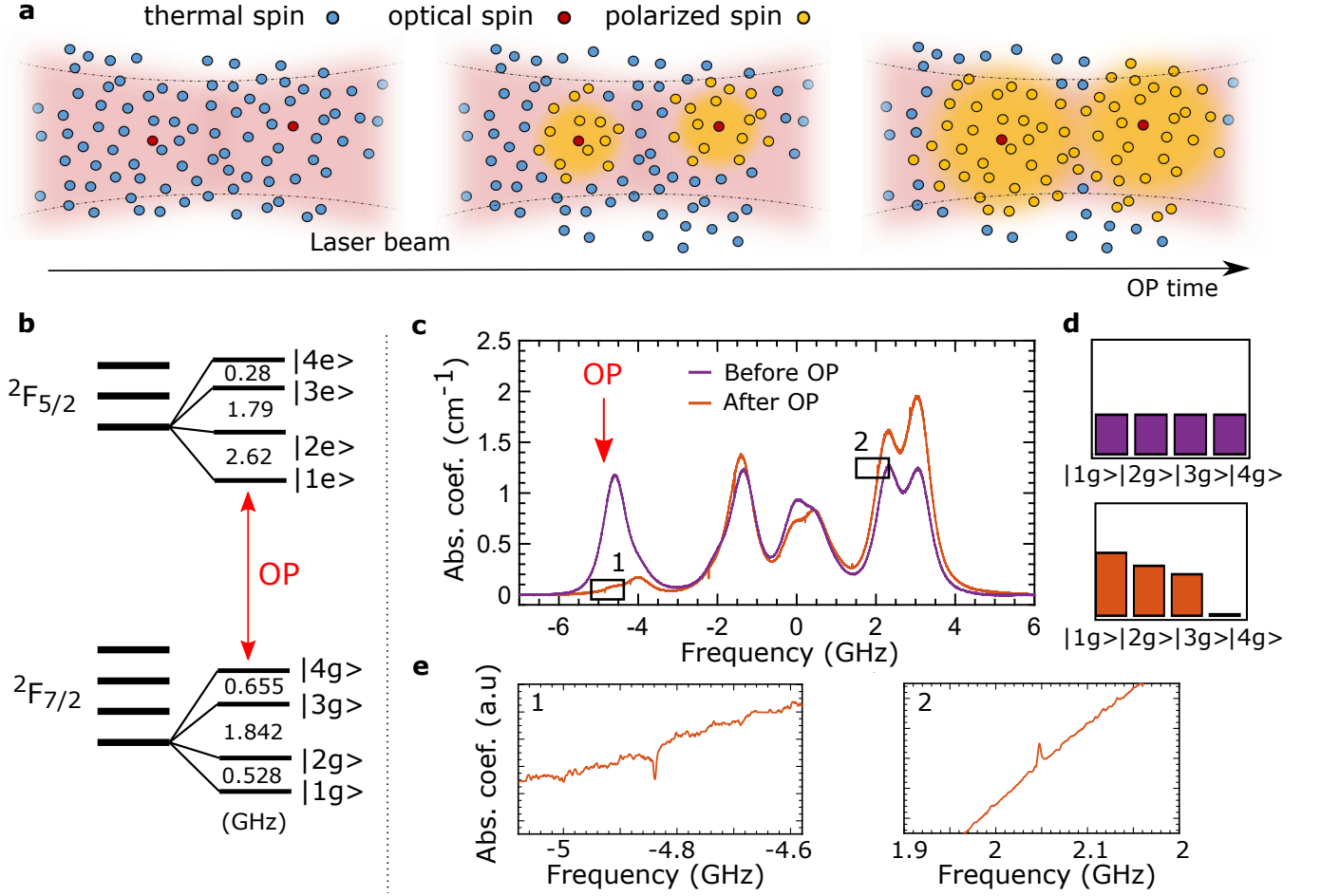


FIG. 1: Diffusion Enhanced Optical Pumping (DEOP) in $^{171}\text{Yb}^{3+}:\text{Y}_2\text{SiO}_5$. **a** DEOP mechanism: optically pumped spins (red circles) initially surrounded by spins in thermal equilibrium (blue circles) gradually polarize neighboring and further apart spins (yellow circles) through flip-flop interactions. **b** Energy diagram showing the $^{171}\text{Yb}^{3+}$ hyperfine structure. **c** Absorption spectrum without (purple) and after 20 s of optical pumping (orange). The OP is along the $|4g\rangle \rightarrow |1e\rangle$ transition (red arrow in **b,c**). **d** Ground state spin populations k_{ig} , normalized by thermal equilibrium values, over the volume addressed by the laser without OP (top, purple, $k_{ig} = 1$) and after OP (bottom, orange, $k_{1g}, k_{2g}, k_{3g}, k_{4g} = 1.67 \pm 0.30, 1.28 \pm 0.36, 1.01 \pm 0.12, 0.04 \pm 0.04$). **e** Enlarged regions 1 and 2 in **c** showing a narrow hole at the laser frequency ($|4g\rangle \rightarrow |1e\rangle$) and a corresponding antihole ($|2g\rangle \rightarrow |3e\rangle$).

other materials. It paves the way to applications of concentrated, optically active, spin ensembles such as multimode optical or microwave quantum memories and high sensitivity magnetic sensing.

I. RESULTS

Experiments were performed using a 10 ppm $^{171}\text{Yb}^{3+}:\text{Y}_2\text{SiO}_5$ (YSO) single crystal sample (see Methods). $^{171}\text{Yb}^{3+}$ has 1/2 electron and nuclear spins and the corresponding ground ($^2F_{7/2}$) and excited state ($^2F_{5/2}$) hyperfine structures, for ions in site 2, are presented in Fig. 1b. The optical transition is centered at 978.854 nm (vac.). Due to anisotropic Zeeman and hyperfine interactions, all hyperfine levels are non-degenerate and their states show completely symmetric superposition of electron and nuclear spin projections. This results in levels that are insensitive to magnetic field fluctuations at first order under zero external magnetic field. Coherence lifetimes of all transitions are thus significantly enhanced for very low magnetic fields, reaching up to 4 ms and 180 μs for spin and optical transitions at 3 K¹⁷.

A. Optical pumping

Diffusion Enhanced Optical Pumping (DEOP) was studied at 2 K. A narrow linewidth (about 1 MHz) laser excited the ${}^2F_{7/2} \rightarrow {}^2F_{5/2}$ transition for a few 10s of seconds. The laser was then blocked for a few ms to let the excited state population relax to the ground state and finally, with a reduced power, shone again on the sample and frequency scanned to determine ${}^{171}\text{Yb}^{3+}$ absorption spectrum (see Methods). In many crystals, RE spins can be optically pumped at low temperature since excitation to the optical state and subsequent decay often result in population transfer between ground state spin levels. Since the laser linewidth is usually much narrower than the RE optical inhomogeneous linewidth, optical pumping creates spectral holes and anti-holes in transmission spectra, i.e. regions of low and high absorption that can be as narrow as twice the optical homogeneous linewidth^{20,35}.

In ${}^{171}\text{Yb}^{3+}:\text{YSO}$, spectral hole burning is not the only phenomenon that occurs. Indeed, as shown in Fig. 1c, after pumping for 20 s the $|4g\rangle \leftrightarrow |1e\rangle$ transition with a 1 MHz linewidth laser, the whole 550 MHz inhomogeneously broadened line vanished. This means that essentially all spins in the sample volume addressed by the laser that were initially in the $|4g\rangle$ state ($\approx 2 \times 10^{14}$ spins) have been transferred to other spin states, despite only 0.4 % of these spins being optically excited. The fraction of excited ions is determined from the overlap between the absorption spectrum and the laser lineshape (see Methods). An analysis of the absorption spectrum, based on previously determined energies and branching ratios of transitions between ground and excited state spin levels, allowed us to accurately determine ground state spin level populations (^{31,36} and see SI for details). This analysis shows that only 4 % of the initial population is left in $|4g\rangle$ (Fig. 1d). We also note in Fig. 1c,e that holes and anti-holes can be observed, although with a low contrast, in the spectrum. They reveal the narrow homogeneous linewidth of the optical transition. The frequency positions of the holes and anti-holes correspond to the pattern expected under spectral hole burning³¹, ruling out spurious effects like large laser drifts during optical pumping.

As explained in the introduction, we attribute this large spin polarization to energy exchanges by flip-flop between ${}^{171}\text{Yb}^{3+}$ ground state spins. This process leads to a diffusion of the population imbalance imposed by the optical pumping of a small fraction of the spins. RE ions are randomly distributed over the volume of the crystal and their optical frequencies, determined by local strains, are not expected to be correlated with their location³⁷. Ions resonant at a given optical frequency are therefore distributed over the volume addressed by the laser, which results, under optical pumping, in a macroscopic spatial spin population gradient and in turn population diffusion, as illustrated in Fig. 1a and SI. The observation of a decrease of the overall optical absorption also indicates the absence of strong correlation between optical and spin transition frequencies.

An important goal of this study was to quantify how the degree of polarization depends on the fraction of optically pumped ions, as well as the characteristic time required to reach that polarization. To this end we varied the optical pumping frequency across the $|4g\rangle \leftrightarrow |1e\rangle$ transition and recorded absorption spectra for different pumping durations τ_P . Fig. 2a shows the region of the absorption spectrum corresponding to the $|4g\rangle \leftrightarrow |1e\rangle$ transition, centered at zero frequency detuning, with a smaller contribution from the $|3g\rangle \leftrightarrow |1e\rangle$ transition at +0.65 GHz. The laser frequency is set at -0.17 GHz, as shown by the hole that appears on spectra recorded for pump durations $1 \leq \tau_P \leq 25$ s. When τ_P is increased, the whole inhomogeneously broadened absorption decreases, without change in shape, and reaches a plateau after about $\tau_P = 30$ s. From the peak absorption coefficient, measured at 0 GHz in Fig. 2a, we deduce k_{4g} , which is level $|4g\rangle$ population normalized by its value without pumping, i.e. at thermal equilibrium (see Methods and SI). The same experiment was repeated for different laser frequencies, shown by the arrows on Fig. 2a, which effectively reduce the fraction of optically pumped spins. The corresponding variations of k_{4g} are displayed in Fig. 2b.

As the laser moves away from the peak absorption of the $|4g\rangle \leftrightarrow |1e\rangle$ transition, k_{4g} decreases more slowly as a function of τ_P and plateaus at a higher value. We found that it could be well fitted by an exponential expression of the form $k_{4g} = \exp(-R_P \tau_P) + k_{4g}^\infty$.

Fig. 2c shows the variation of the steady-state population k_{4g}^∞ and the polarization rate R_P as a function of the fraction C of optically pumped ions, determined from the overlap between the absorption spectrum and laser lineshape (see Methods). The variation of R_P and k_{4g}^∞ can be understood in the following way: when C decreases, each pumped spin has to polarize a larger number of non-pumped spins to reach a given k_{4g} value; this slows down the overall spin diffusion and decreases the polarization rate R_P . The degree of achievable spin polarization is limited by the interaction of individual spins with the phonon bath, so-called spin lattice relaxation (SLR), which will counteract DEOP. Hence, the steady-state population k_{4g}^∞ is determined by the balance between SLR and spin diffusion rates, such that a smaller R_P (and thus C) implies a larger k_{4g}^∞ . At the highest fraction of pumped ions, $C = 5.8 \times 10^{-3}$, $k_{4g}^\infty = 0.08 \pm 0.02$ and $1/R_P = 3 \pm 0.6$ s, which increases to $k_{4g}^\infty = 0.74 \pm 0.02$ and $1/R_P = 91 \pm 27$ s for $C = 2 \times 10^{-4}$, the lowest value investigated. Even by pumping such a small fraction of ions, 25% of $|4g\rangle$ spins are transferred to another level, showing the efficiency of DEOP in this system.

The data in Fig. 2c suggest that R_P depends linearly on C whereas k_{4g}^∞ varies as $1/C$. This can be accounted

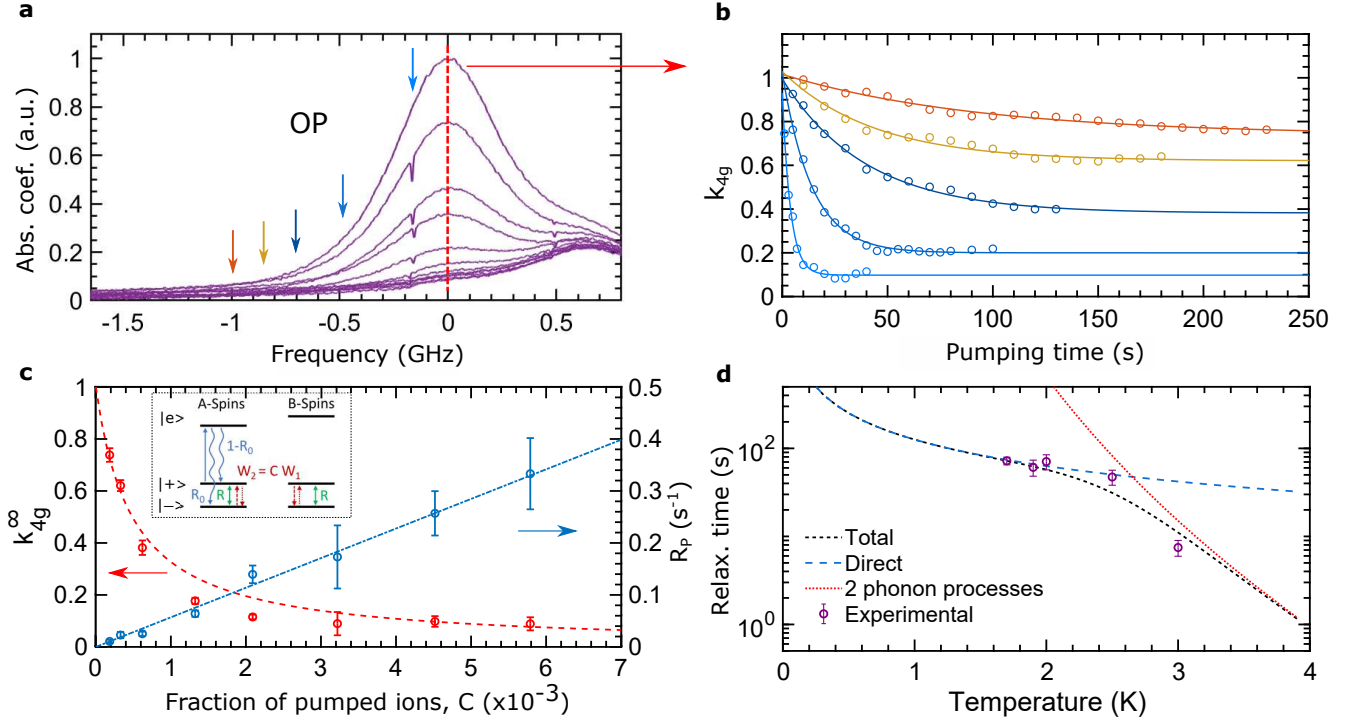


FIG. 2: Dynamics of DEOP and spin-lattice relaxation. **a** Absorption profile around the $|4g\rangle \leftrightarrow |1e\rangle$ transition after 0 s, 1 s, 3 s, 5 s, 7 s, and every 5 s from 10 s to 40 s of OP at -0.17 GHz (light blue arrow). The whole inhomogeneously broadened absorption decreases when pumping duration increases. The laser creates a narrow spectral hole at -0.17 GHz clearly seen for pump duration between 1 and 7 s. The small side hole at +0.5 GHz originates from the $|3g\rangle$ level and should therefore appear as an antihole. This is explained by a fast relaxation between the $|4g\rangle$ and $|3g\rangle$ levels by flip-flop processes³¹. The absorption centered at +0.66 MHz corresponds to the $|3g\rangle \leftrightarrow |1e\rangle$ transition. **b** Normalized level $|4g\rangle$ population k_{4g} as a function of OP duration for different laser frequencies shown in **a** by color-coded arrows. Solid lines are exponential fits to the data (see text). **c** Level $|4g\rangle$ normalized steady state populations (k_{4g}^∞) and polarization rate (R_P) as a function of the fraction of pumped ions (see text). Solid lines correspond to fits using a spin 1/2 model and rate equations. Inset: Spin 1/2 model scheme (see text). **d** Spin lattice relaxation time as a function of temperature deduced from absorption recovery after OP is stopped. Solid lines are fits using direct and two-phonon processes (see text). All error bars correspond to a 95% confidence interval.

for by a simple model that treats $^{171}\text{Yb}^{3+}$ ions as an ensemble of 1/2 spins divided into two groups: the A-spins are optically pumped to their ground state; the B-spins are not pumped but are expected to polarize to their lower state through DEOP (Fig. 2c, inset). C is therefore the ratio between A and B-spin concentrations. We use rate equations to describe the individual relaxations as well as the flip-flop processes between A and B-spins (see SI for details). They can be solved analytically, leading to

$$k_{4g}^\infty \equiv p_B^{+, \infty} \approx \frac{1}{2 + C\beta_{ff}/\beta_o} \quad (1)$$

$$R_P \approx R(2 + C\beta_{ff}/\beta_o), \quad (2)$$

where p_B^+ is B-spins upper state population and R the spin-lattice relaxation rate. These expressions have indeed the correct dependence on C with respect to experimental observations. $\beta_{ff} = W_1/(W_1 + R_o)$ and $\beta_o = R/R_o$, where R_o is A-spins effective optical pumping rate (Fig. 2c, inset). W_1 is the relaxation rate of A-spins by flip-flop with B-spins and $W_2 = CW_1$ is the relaxation rate of B-spins by flip-flop with A spins.

As shown in Fig. 2c, reasonable agreement was obtained when fitting experimental k_{4g}^∞ and R_P using Eqs. (1) and (2), which indicates that a two-level system can be indeed used to model $^{171}\text{Yb}^{3+}$ under these DEOP conditions. Theoretical flip-flop rates show that this is possible due to the fast flip-flops that occur within the $|1g\rangle - |2g\rangle$ and $|3g\rangle - |4g\rangle$ pair of levels (see SI). In this case, each pair of levels can be grouped and considered as one level, leading to an effective 1/2 system. Flip-flops within others pairs of levels, like $|4g\rangle - |2g\rangle$, are much slower. W_1 corresponds to these slow rates, as they are found to be the limiting interaction for B spins polarization. With the additional assumption $R_o \gg W_1$, Fig. 2c fits give $W_1 = 57 \pm 5 \text{ s}^{-1}$ and $R = (1.4 \pm 0.4) \times 10^{-2} \text{ s}^{-1}$. We estimate $R_o = 384 \text{ s}^{-1}$ from excited state lifetime and optical branching ratios, and $W_1 = 13 \text{ s}^{-1}$ from narrow hole decays (see SI). These qualitative

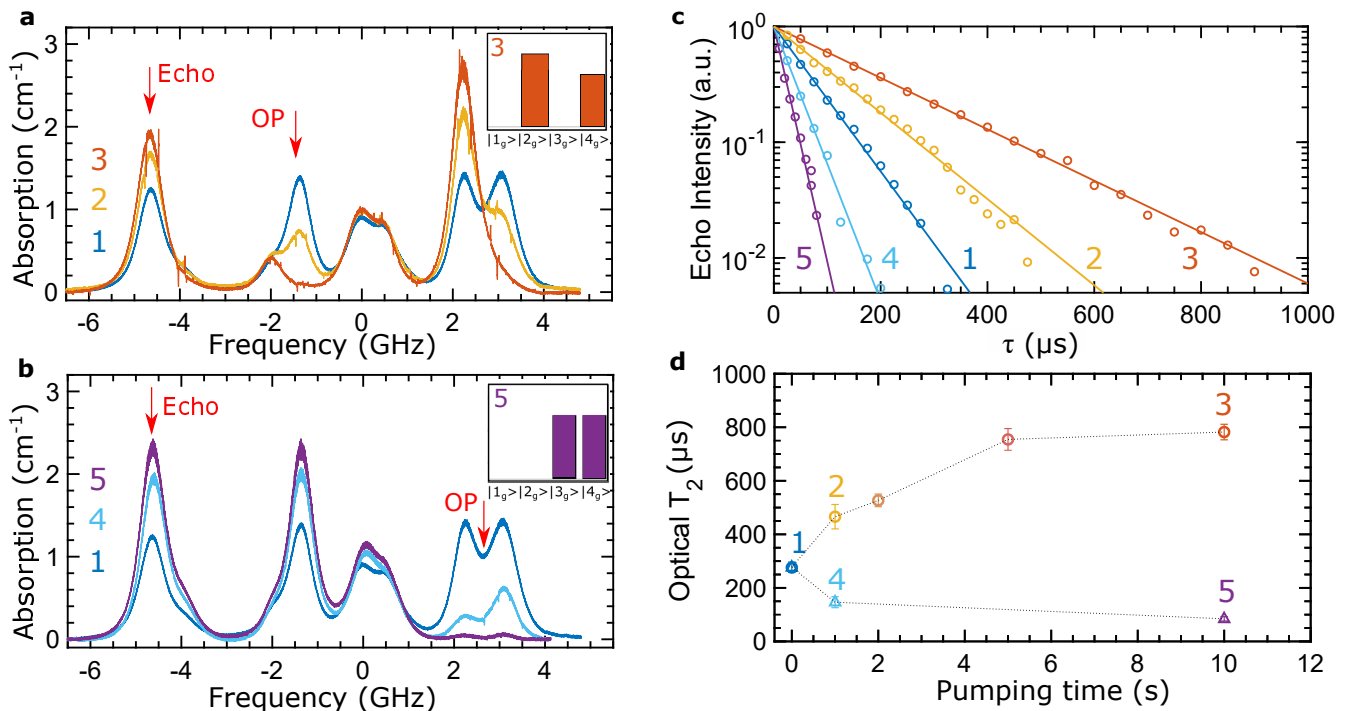


FIG. 3: Optical coherence lifetime under DEOP. **a** Absorption spectra after 0, 1 and 10 s of OP at -1.44 GHz. Inset: normalized ground state populations $k_{1g}, k_{2g}, k_{3g}, k_{4g} = 0.02 \pm 0.02, 2.30 \pm 0.12, 0.02 \pm 0.02, 1.70 \pm 0.06$. **b** Absorption spectra after 0, 1 and 10 s of OP at +2.67 GHz. Inset: normalized ground state populations $k_{1g}, k_{2g}, k_{3g}, k_{4g} = 0.02 \pm 0.02, 0.02 \pm 0.02, 1.95 \pm 0.10, 2.05 \pm 0.08$. **c** Photon echo decays under DEOP for the $|4g\rangle \leftrightarrow |1e\rangle$ transition measured at -4.6 GHz (arrow in **a**, **b**). Decay colors and numbers correspond to spectra in **a**, **b**, solid lines are exponential fits to the data. **d** Optical coherence times $T_{2,o}$ deduced from fits in **c** (color-coded). All error bars correspond to a 95% confidence interval.

agreements support our simple spin 1/2 level-rate equation approach. However, we expect that when transitions connecting different ground state levels are simultaneously pumped (see section IB), a more complex 4-level-modeling is necessary.

We finally recorded the $|4g\rangle \leftrightarrow |1e\rangle$ absorption spectra at different delays after DEOP. As in the previous experiments, the line shape did not change while the initial absorption was gradually recovered, and the peak absorption coefficient allowed us to monitor level $|4g\rangle$ population over all the spins in the volume addressed by the laser. Since flip-flops do not change overall level populations, the recovery rate R_c , obtained by an exponential fit to the data, corresponds to the SLR rate. This is confirmed by R_c temperature dependence shown in Fig. 2d which can be well modeled by a sum of a direct process and 2-phonon processes, with parameters consistent with previous studies at higher magnetic field³², as detailed in SI. At 2 K, the temperature used for DEOP experiments, $R_c = 1/(72 \text{ s}) = 1.4 \times 10^{-2} \text{ s}^{-1}$, in qualitative agreement with the fitted value $2R = (2.8 \pm 0.8) \times 10^{-2} \text{ s}^{-1}$.

B. Optical coherence

We next investigated optical coherence lifetimes, $T_{2,o}$ under DEOP. This was motivated by several studies that have shown that flipping ground state spins of paramagnetic RE can be a major source of magnetic noise and therefore cause dephasing to RE optical and spin transitions^{8,32}. This can be reduced by inducing strong spin polarization under large magnetic field and/or ultra-low temperatures, broadband optical pumping or using excited state spins^{13,14,29,38,39}. As shown in the previous section, DEOP also induces large scale spin polarization and could therefore achieve similar effects.

Optical coherence lifetimes were measured for the $|4g\rangle \leftrightarrow |1e\rangle$ transition under several DEOP conditions. In a first series of measurements, DEOP was performed with a laser set at -1.44 GHz in the spectrum displayed in Fig. 3a. At this frequency, some ions are pumped along the $|1g\rangle \leftrightarrow |1e\rangle$ transition and others along the $|3g\rangle \leftrightarrow |2e\rangle$ one because of the overlap between these inhomogeneously broadened lines. This results in progressively pumping away the populations of the $|1g\rangle$ and $|3g\rangle$ levels when the DEOP duration is increased (Fig. 3a). After 10 s, nearly all

the initial populations of these two levels have been transferred to $|4g\rangle$ and $|2g\rangle$. A second DEOP configuration was studied, setting the laser frequency at +2.67 GHz (Fig. 3c). In this case, the optical excitation is resonant with the four optical transitions $|1g\rangle \leftrightarrow |3e\rangle$, $|1g\rangle \leftrightarrow |4e\rangle$, $|2g\rangle \leftrightarrow |3e\rangle$ and $|2g\rangle \leftrightarrow |4e\rangle$. As a result, the states $|1g\rangle$ and $|2g\rangle$ are now emptied, and $|3g\rangle$ and $|4g\rangle$ filled, when DEOP is applied (Fig. 3b). These two configurations highlight the versatility of DEOP that allow polarizing spins in different levels and not only in the lowest energy one, as would result from using large magnetic fields or low temperatures.

For each laser frequency and DEOP duration, the optical coherence time of the $|4g\rangle \leftrightarrow |1e\rangle$ transition was measured with photon echoes (see Methods). The echo decays obtained by varying the delay between the excitation and rephasing pulses are displayed in Fig. 3c. Decay rates show large variations as a function of DEOP conditions and corresponding coherence lifetimes $T_{2,o}$, obtained by single exponential fits, are gathered in Fig. 3d. Without DEOP, $T_{2,o} = 278 \pm 20 \mu\text{s}$ or $\Gamma_{h,o} = 1/\pi T_{2,o} = 1.1 \pm 0.1 \text{ kHz}$. It reaches $782 \pm 30 \mu\text{s}$ after 10 s of DEOP that empties the $|1g\rangle$ and $|3g\rangle$ levels (Fig. 3a,d). The corresponding homogeneous linewidth is $\Gamma_{h,o} = 407 \pm 15 \text{ Hz}$. This is the narrowest homogeneous linewidth reported at zero magnetic field for any RE, with the exception of non-Kramers $\text{Eu}^{3+}:\text{Y}_2\text{SiO}_5$ in which linewidths $< 290 \text{ Hz}$ have been measured⁴⁰.

When DEOP is used to empty $|1g\rangle$ and $|2g\rangle$ levels, a very different result is observed: $T_{2,o}$ is strongly reduced, down to $84 \pm 8 \mu\text{s}$, equivalent to a homogeneous linewidth of $\Gamma_{h,o} = 3.8 \pm 0.4 \text{ kHz}$. This is a factor of ten difference as compared to the first DEOP configuration, and about 3.5 times the value obtained without pumping. To the best of our knowledge, this is the first demonstration of changes, and especially significant enhancement, in coherence lifetime induced by optical pumping. This is especially significant for systems that should be used at low magnetic field, to take advantage of magnetic insensitive transitions¹⁵, as here in $^{171}\text{Yb}^{3+}:\text{Y}_2\text{SiO}_5$, or when constraints from other devices such as superconducting resonators are relevant.

Contributions to the $|4g\rangle \leftrightarrow |1e\rangle$ homogeneous linewidth can be expressed in terms of levels $|4g\rangle$ and $|1e\rangle$ populations lifetimes T_1 and pure dephasing Γ_ϕ as:

$$\Gamma_{h,o} = \frac{1}{2\pi T_{1,4g}} + \frac{1}{2\pi T_{1,1e}} + \Gamma_\phi. \quad (3)$$

The excited-state lifetime $T_{1,1e}$ can be taken to be simply its radiative lifetime, $T_{1,1e} = T_{1,o} = 1.3 \text{ ms}$, hence independent of DEOP, as SLR rates on the same order than in the ground state (close hyperfine and crystal field splittings^{30,31}) and the spin flop-flop rates are negligible due to the low concentration of excited ions. For the ground state we also disregard SLR contributions to $T_{1,4g}$, as the estimated SLR lifetime is $\approx 2/R_c = 144 \text{ s}^{-1}$. However, the flip-flop rates can contribute to $\Gamma_{h,o}$ both directly through the $T_{1,4g}$ lifetime and indirectly through the dephasing term Γ_ϕ . The contribution to Γ_ϕ is then a spectral diffusion process, where flip-flops in the $^{171}\text{Yb}^{3+}$ spin bath create a time-varying magnetic field noise on the optically probed ion.

Both the direct and indirect flip-flop contributions are expected to change through DEOP. Our calculations of the flip-flop rates between ions in different hyperfine states show that the highest rates are due to flip flops in between ions in $|1g\rangle$ and $|2g\rangle$, and $|3g\rangle$ and $|4g\rangle$, respectively (see SI). Hence, we expect that the flip flop rate will strongly decrease when ions are pumped into states $|2g\rangle$ and $|4g\rangle$ using DEOP, as in Fig. 3a. Conversely we expect the flip flop rate to strongly increase when ions are pumped into states $|3g\rangle$ and $|4g\rangle$ using DEOP, as in Fig. 3b. This qualitatively explains the change in coherence time due to DEOP, as seen in Figs 3c and 3d. However, these data are not sufficient to distinguish between the direct (lifetime) and indirect (spectral diffusion) contributions to the coherence time.

To this end, we also performed spin coherence measurements on the $|3g\rangle \leftrightarrow |4g\rangle$ transition at 655 MHz, as described in the SI. For this, we polarized a large fraction of the spins into either the $|1g\rangle$ and $|2g\rangle$ states, or the $|3g\rangle$ and $|4g\rangle$ states, respectively. In both cases the populations in these two levels were essentially the same. An indirect spectral diffusion contribution to the spin coherence lifetime would be roughly equal in both cases, as the flip-flop rates are expected to be the same for both cases (see flip-flop calculations in SI). However, the direct lifetime contribution to the probed states $|3g\rangle$ and $|4g\rangle$ would strongly decrease when spins are polarized into $|1g\rangle$ and $|2g\rangle$ states, as the spin flip-flop probability of spins in both the $|3g\rangle$ and $|4g\rangle$ states would be reduced. Indeed, we observed a strong change in spin coherence lifetime for the two cases, going from 0.2 to 2.5 ms as spins are polarized into $|1g\rangle$ and $|2g\rangle$ states.

The spin coherence measurements indicate that direct flip-flop lifetimes significantly contribute to the optical coherence lifetimes in 10 ppm doped $^{171}\text{Yb}^{3+}:\text{Y}_2\text{SiO}_5$. Strong spin polarization using DEOP into selected hyperfine states can strongly reduce this contribution, as well as indirect contributions, to optical and spin dephasing. The data in Fig. 3d show that the DEOP effect is saturated for the longest pumping time, which suggests that direct and indirect contributions have been largely quenched. This allows to estimate the dephasing contribution to Γ_ϕ independent from DEOP to 285 Hz. Presumably, $^{171}\text{Yb}^{3+}$ in site 1, which represent 50% of the total Yb^{3+} concentration, cause a significant part of this broadening. It could be reduced to a large extent by using DEOP on these ions using e.g. a second laser. In this case, the remaining dephasing would be interactions with $^{89}\text{Y}^{3+}$. Since the latter are very slow⁸, it could be possible to reach the $T_{2,o} = 2T_{1,o}$ limit.

Although this qualitative analysis can account for the general trends observed, a more detailed modeling and additional experiments are needed to precisely evaluate the processes affecting $T_{2,o}$. In particular, all ground state flip-flops should be included in simulations and their rates determined using spectral hole burning or other techniques. Further theoretical calculations of flip-flop rates and frequency shifts caused by spin flips could also be very useful.

II. DISCUSSION

The spin 1/2 rate equation model (Eqs. 1-2) is convenient to estimate parameters for efficient DEOP, i.e. low remaining population in B-spin upper level, $p_B^{+, \infty}$. First, low values of $\beta_o = R/R_o$ are required and therefore small SLR rate R and/or strong optical pumping, i.e. larger R_o . The latter may be limited, as in our case, by the spontaneous emission rate and branching ratios, which in turn can be increased using optical nano-cavities^{26,27,41}. Small R values can be achieved by lowering magnetic field and temperature⁸. This is the case in our experiments, running at 2 K and zero magnetic field, giving $\beta_o \approx 3.6 \times 10^{-5}$ and polarizations over 90%. However, SLR increases quickly with temperature or magnetic field, and Fig. 2d modeling predicts that at 4 K and zero field DEOP polarizes only 11% of the spins. Large β_{ff} is also favorable and corresponds to strong flip-flops, i.e. large W_1 . This can be obtained with high spin concentration n_0 and lower inhomogeneous linewidth since $W_1 \propto n_0^2/\Gamma_{inh,spin}$ ⁸. In $^{171}\text{Yb}^{3+}:\text{Y}_2\text{SiO}_5$, it is worth noting that the spin linewidth is especially narrow at zero magnetic field, $\Gamma_{inh,spin} = 1$ MHz¹⁷, which increases flip-flop rates and gives $\beta_{ff} \approx 0.13$. Finally, pumping a larger fraction of ions will obviously result in stronger polarization by increasing C . However, as demonstrated in our experiments, low C values can still provide strong polarization. The case when more than one transition is optically pumped, as investigated in the 'Optical Coherence' section is more difficult to analyze with a simple 1/2 spin model. Non-pumped spins will interact with several classes of optically pumped spins that are polarized in different levels. This can lead to high polarization, as we observed, but also to opposite population changes and therefore remaining populations in some pumped levels. In this respect, isolated optical transitions, like the $|4g\rangle \leftrightarrow |1e\rangle$ in $^{171}\text{Yb}^{3+}:\text{Y}_2\text{SiO}_5$ simplify pumping schemes and will appear for spin splittings at least comparable to the optical inhomogeneous linewidth. While this can often be obtained with a high enough magnetic field, it may also increase SLR through direct processes and lower flip-flop rates by increasing spin inhomogeneous linewidth^{39,42}, effects that both reduce DEOP.

This study suggests that efficient DEOP could be observed in other paramagnetic RE or transition metal ions doped materials. DEOP was observed in $\text{Cr}^{3+}:\text{Al}_2\text{O}_3$ ³⁴ and can also be seen in $\text{Nd}^{3+}:\text{YVO}_4$ as shown in Fig. 5 of Ref.⁴³, although it was not recognized as such in this work. It could especially be observed in other candidates of interest for applications in quantum technologies including Er^{3+} , although this ion suffers from inefficient optical pumping which increases the requirement on low SLR⁴⁴. Paramagnetic RE with non zero nuclear spins that show ground state splittings of a few GHz at zero magnetic field such as $^{167}\text{Er}^{3+}$, $^{145}\text{Nd}^{3+}$ or $^{173}\text{Yb}^{3+}$ could also behave similarly to $^{171}\text{Yb}^{3+}$ for DEOP. Finally, other concentrated spin systems with optical transitions, such as NV^- centers in diamond, could also show DEOP.

Using DEOP, we managed to reduce by 250% the optical homogeneous linewidths, to get a value of $\Gamma_{h,o} = 407 \pm 15$ Hz, which is the narrowest homogeneous linewidth reported at zero magnetic field for any RE, except for $\text{Eu}^{3+}:\text{Y}_2\text{SiO}_5$ ⁴⁰. However, Eu^{3+} only possesses nuclear degrees of freedom and its ground state nuclear hyperfine structure spans only 60 to 160 MHz in this crystal, depending on the isotope⁴⁵. This is about 20 times less than $^{171}\text{Yb}^{3+}$ (3 GHz), which in addition has 3×10^6 times stronger spin transition dipole moments¹⁷. $^{171}\text{Yb}^{3+}$ is therefore much better suited for interactions with microwave photons while showing comparable optical coherence lifetimes.

As it is the case for $^{171}\text{Yb}^{3+}:\text{Y}_2\text{SiO}_5$, DEOP could extend optical and/or spin coherence lifetimes of other solid state systems by reducing spin-spin interactions. It therefore allows keeping a high concentration of active species with low dephasing. This is a particularly important point for ensemble based quantum devices, like absorptive quantum memories that require high optical absorption⁴⁶. In addition, various configurations of populated levels can be in principle obtained, allowing to select the best configurations for e.g. strong optical and spin transitions, long coherence lifetimes, long lived shelving states etc. DEOP can also provide large scale spin initialization prior to cohering and/or spectral tailoring. As an example, we achieved $96 \pm 1\%$ polarization in the single $|4g\rangle$ level of $^{171}\text{Yb}^{3+}:\text{Y}_2\text{SiO}_5$ (see SI). Finally, in the case of systems with different sites for optically addressable spins, a common feature in rare-earth doped crystals, it can also lower the perturbations from the unused centers.

In conclusion, we have observed large-scale spin polarization under laser excitation at fixed frequency in a rare earth doped crystal, $^{171}\text{Yb}^{3+}:\text{Y}_2\text{SiO}_5$. This is explained by a combination of optical pumping and spin diffusion by flip-flops that results in $> 90\%$ polarization for all spins in the sample volume addressed by the laser. The efficiency and versatility of the process is furthermore demonstrated by significantly increasing and decreasing optical coherence lifetimes $T_{2,o}$, depending on the pumping conditions. The longest $T_{2,o}$ recorded, $\approx 800\mu\text{s}$, is the longest recorded for a paramagnetic RE at zero magnetic field and is comparable to values for non-paramagnetic RE. Given the other favorable optical and spin properties of $^{171}\text{Yb}^{3+}:\text{Y}_2\text{SiO}_5$, our results open the way to new designs for broadband and

efficient quantum memories for light³⁶ or optical to microwave transducers. We expect this process to be efficient in other rare earth doped crystals and concentrated systems of optically addressable spins like color centers in diamond. It could be used to tailor spin baths and therefore extend coherence lifetimes, or initialize spins on a large scale, topics which are central to many quantum technologies.

III. ACKNOWLEDGEMENTS

This project has received funding from the European Union's Horizon 2020 research and innovation programme under grant agreement No 71272, the IMTO Cancer AVIESAN (Cancer Plan, C16027HS, MALT) and FNS Research Project No 172590.

IV. AUTHOR CONTRIBUTIONS

S.W. and A.F. grew the sample, S.W. and P.G. conceived and performed the experiments, except for the additional spin coherence measurements which were performed by M. B. and A. T.. S.W., P.G., M.A., A.T. and M.B analyzed the results, and S.W. and P.G. wrote the manuscript with inputs from all co-authors. P.G. and M.A. provided overall oversight of the project.

V. METHODS

A. Sample

The Y_2SiO_5 single crystal was doped with 10 ppm of $^{171}\text{Yb}^{3+}$ (94% isotopic purity, see SI) and grown by the Czochralski technique. It was cut along the extinction axis b , D_1 and D_2 , with light propagating along the b axis and polarized along D_2 for maximal absorption. The length of the sample along b was 9.4 mm. Y_2SiO_5 has a monoclinic structure and belongs to the C_{2h}^6 space group. Yb^{3+} can substitute Y^{3+} ions equally in their two sites of C_1 point symmetry.

B. Experimental setup and optical pumping

The sample was placed inside a liquid helium bath cryostat at 2 K. Excitation was provided by a tunable single mode diode laser (Toptica DL 100) with a spectral width of 1 MHz. The beam on the sample was weakly focused on the sample with a diameter of 1 mm. All experiments were performed in transmission mode. Spectra were calibrated by recording signal from a Toptica FPI 100 Fabry-Perot interferometer (1 GHz free spectral range). An acousto-optic modulator (AOM, AA Optoelectronics MT80) in single pass configuration was used to gate the laser. The detector was an amplified Si photodiode (Thorlabs PDA150A). The power during optical pumping and scans was 7 mW and 0.4 mW, with frequency scans performed at a rate of 3 GHz/ms. A delay of 10 ms was kept between optical pumping and scanning to let the excited state population decay to the ground state. To probe absorption recovery, scans were performed at different delays after 20 s of optical pumping and at different temperatures.

Fraction of pumped ions are calculated from absorption spectrum using the formula

$$C = \frac{2}{\pi} \frac{\Gamma}{\Gamma_0} \frac{\alpha}{\alpha_0}, \quad (4)$$

where α and α_0 are absorption coefficients at the laser frequency and peak of the line, Γ_0 the full width at half maximum and Γ the pumped region spectral width. We have $\Gamma_0 = 550 \text{ MHz}^{17}$ and $\Gamma \approx 5 \text{ MHz}$. The latter value corresponds to the hole observed on the absorption spectra and takes into account the laser linewidth (1 MHz), drift and other effects like power broadening.

In Fig. 2a, the absorption lineshape does not change with pumping duration and the fraction of pumped ions is small. The peak absorption coefficient measured at 0 GHz and normalized by its value without OP, i.e. at thermal equilibrium, is therefore equivalent to k_{4g} .

C. Optical coherence measurement

For those measurements, a second AOM was added to enhance gating and avoid optical pumping during photon echo sequences. The beam was focused by a 100 mm focal length lens with a power of 7 mW. The photon echo was measured using a standard Hahn echo sequence ($\pi/2 - \tau - \pi - \tau - \text{echo}$) with durations of 1 and 2 μs for the $\pi/2$ and π pulses. Due to the laser jitter, the echo amplitude significantly fluctuated for $\tau > 300 \mu\text{s}$. To overcome this issue, for a given delay τ , 50 successive echo sequences were recorded and only the strongest echo was kept. We checked that the echo sequences themselves did not cause optical pumping. Echo pulse power was also varied to look for instantaneous spectral diffusion, which was not observed.

-
- * Present affiliation : Department of Electrical Engineering, Princeton University, Princeton, NJ 08544, USA
 † Present affiliation : The Niels Bohr Institute, University of Copenhagen, DK-2100 Copenhagen Ø, Denmark
 ‡ philippe.goldner@chimieparistech.psl.eu
- ¹ M. Atatüre, D. Englund, N. Vamivakas, S.-Y. Lee, and J. Wrachtrup, Material platforms for spin-based photonic quantum technologies, *Nat. Rev. Mater.* **3**, 1 (2018).
 - ² F. Bussi eres, C. Clausen, A. Tiranov, B. Korzh, V. B. Verma, S. W. Nam, F. Marsili, A. Ferrier, P. Goldner, H. Herrmann, C. Silberhorn, W. Sohler, M. Afzelius, and N. Gisin, Quantum teleportation from a telecom-wavelength photon to a solid-state quantum memory, *Nat. Photonics* **8**, 775 (2014).
 - ³ B. Hensen, H. Bernien, A. E. Dr eau, A. Reiserer, N. Kalb, M. S. Blok, J. Ruitenber, R. F. L. Vermeulen, R. N. Schouten, C. Abell an, W. Amaya, V. Pruneri, M. W. Mitchell, M. Markham, D. J. Twitchen, D. Elkouss, S. Wehner, T. H. Taminiau, and R. Hanson, Loophole-free Bell inequality violation using electron spins separated by 1.3 kilometres, *Nature* **526**, 682 (2015).
 - ⁴ H. J. Kimble, The quantum internet, *Nature* **453**, 1023 (2008).
 - ⁵ J. M. Boss, K. S. Cujia, J. Zopes, and C. L. Degen, Quantum sensing with arbitrary frequency resolution, *Science* **356**, 837 (2017).
 - ⁶ M. Zhong, M. P. Hedges, R. L. Ahlefeldt, J. G. Bartholomew, S. E. Beavan, S. M. Wittig, J. J. Longdell, and M. J. Sellars, Optically addressable nuclear spins in a solid with a six-hour coherence time, *Nature* **517**, 177 (2015).
 - ⁷ D. Serrano, J. Karlsson, A. Fossati, A. Ferrier, and P. Goldner, All-optical control of long-lived nuclear spins in rare-earth doped nanoparticles, *Nat. Commun.* **9**, 2127 (2018).
 - ⁸ T. B ottger, C. W. Thiel, Y. Sun, and R. L. Cone, Optical decoherence and spectral diffusion at 1.5 μm in $\text{Er}^{3+}:\text{Y}_2\text{SiO}_5$ versus magnetic field, temperature, and Er^{3+} concentration, *Phys. Rev. B* **73**, 075101 (2006).
 - ⁹ H. S. Knowles, D. M. Kara, and M. Atat ure, Observing bulk diamond spin coherence in high-purity nanodiamonds, *Nat. Mater.* **13**, 21 (2014).
 - ¹⁰ G. Balasubramanian, P. Neumann, D. Twitchen, M. Markham, R. Kolesov, N. Mizuochi, J. Isoya, J. Achard, J. Beck, J. Tissler, V. Jacques, P. R. Hemmer, F. Jelezko, and J. Wrachtrup, Ultralong spin coherence time in isotopically engineered diamond, *Nat. Mater.* **8**, 383 (2009).
 - ¹¹ A. M. Tyryshkin, S. Tojo, J. J. L. Morton, H. Riemann, N. V. Abrosimov, P. Becker, H.-J. Pohl, T. Schenkel, M. L. W. Thewalt, K. M. Itoh, and S. A. Lyon, Electron spin coherence exceeding seconds in high-purity silicon, *Nat. Mater.* **11**, 143 (2011).
 - ¹² T. B ottger, C. W. Thiel, R. L. Cone, and Y. Sun, Effects of magnetic field orientation on optical decoherence in $\text{Er}^{3+}:\text{Y}_2\text{SiO}_5$, *Phys. Rev. B* **79**, 115104 (2009).
 - ¹³ M. Rancic, M. P. Hedges, R. L. Ahlefeldt, and M. J. Sellars, Coherence time of over a second in a telecom-compatible quantum memory storage material, *Nat. Phys.* **14**, 50 (2017).
 - ¹⁴ N. Kukharchyk, D. Sholokhov, O. Morozov, S. L. Korableva, A. A. Kalachev, and P. A. Bushev, Optical coherence of $^{166}\text{Er}:\text{LiYF}_4$ crystal below 1 K, *New J. Phys.* **20**, 023044 (2018).
 - ¹⁵ E. Fraval, M. J. Sellars, and J. J. Longdell, Method of Extending Hyperfine Coherence Times in $\text{Pr}^{3+}:\text{Y}_2\text{SiO}_5$, *Phys. Rev. Lett.* **92**, 077601 (2004).
 - ¹⁶ G. Wolfowicz, A. M. Tyryshkin, R. E. George, H. Riemann, N. V. Abrosimov, P. Becker, H.-J. Pohl, M. L. W. Thewalt, S. A. Lyon, and J. J. L. Morton, Atomic clock transitions in silicon-based spin qubits, *Nat. Nanotechnol.* **8**, 561 (2013).
 - ¹⁷ A. Ortu, A. Tiranov, S. Welinski, F. Fr owis, N. Gisin, A. Ferrier, P. Goldner, and M. Afzelius, Simultaneous coherence enhancement of optical and microwave transitions in solid-state electronic spins, *Nat. Mater.* **17**, 671 (2018).
 - ¹⁸ L. Viola and S. Lloyd, Dynamical suppression of decoherence in two-state quantum systems, *Phys. Rev. A* **58**, 2733 (1998).
 - ¹⁹ M. Lovri c, D. Suter, A. Ferrier, and P. Goldner, Faithful Solid State Optical Memory with Dynamically Decoupled Spin Wave Storage, *Phys. Rev. Lett.* **111**, 020503 (2013).
 - ²⁰ P. Goldner, A. Ferrier, and O. Guillot-No el, Rare Earth-Doped Crystals for Quantum Information Processing , in *Handbook on the Physics and Chemistry of Rare Earths*, edited by J.-C. G. B unzli and V. K. Pecharsky (Elsevier, Amsterdam, 2015) pp. 1–78.
 - ²¹ E. Saglamyurek, N. Sinclair, J. Jin, J. A. Slater, D. Oblak, F. Bussi eres, M. George, R. Ricken, W. Sohler, and W. Tittel, Broadband waveguide quantum memory for entangled photons, *Nature* **469**, 512 (2011).

- ²² Z.-Q. Zhou, W.-B. Lin, M. Yang, C.-F. Li, and G.-C. Guo, Realization of Reliable Solid-State Quantum Memory for Photonic Polarization Qubit, *Phys. Rev. Lett.* **108**, 190505 (2012).
- ²³ T. Zhong, J. M. Kindem, J. G. Bartholomew, J. Rochman, I. Craiciu, E. Miyazono, M. Bettinelli, E. Cavalli, V. Verma, S. W. Nam, F. Marsili, M. D. Shaw, A. D. Beyer, and A. Faraon, Nanophotonic rare-earth quantum memory with optically controlled retrieval, *Science* **357**, 1392 (2017).
- ²⁴ C. Laplane, P. Jobez, J. Etesse, N. Gisin, and M. Afzelius, Multimode and Long-Lived Quantum Correlations Between Photons and Spins in a Crystal, *Phys. Rev. Lett.* **118**, 210501 (2017).
- ²⁵ A. Walther, L. Rippe, Y. Yan, J. Karlsson, D. Serrano, A. N. Nilsson, S. Bengtsson, and S. Kröll, High-fidelity readout scheme for rare-earth solid-state quantum computing, *Phys. Rev. A* **92**, 022319 (2015).
- ²⁶ A. M. Dibos, M. Raha, C. M. Phenicie, and J. D. Thompson, Atomic Source of Single Photons in the Telecom Band, *Phys. Rev. Lett.* **120**, 243601 (2018).
- ²⁷ T. Zhong, J. M. Kindem, J. G. Bartholomew, J. Rochman, I. Craiciu, V. Verma, S. W. Nam, F. Marsili, M. D. Shaw, A. D. Beyer, and A. Faraon, Optically Addressing Single Rare-Earth Ions in a Nanophotonic Cavity, *Phys. Rev. Lett.* **121**, 183603 (2018).
- ²⁸ L. A. Williamson, Y.-H. Chen, and J. J. Longdell, Magneto-Optic Modulator with Unit Quantum Efficiency, *Phys. Rev. Lett.* **113**, 203601 (2014).
- ²⁹ S. Welinski, P. J. T. Woodburn, N. Lauk, R. L. Cone, C. Simon, P. Goldner, and C. W. Thiel, Electron Spin Coherence in Optically Excited States of Rare-Earth Ions for Microwave to Optical Quantum Transducers, *Phys. Rev. Lett.* **122**, 247401 (2019).
- ³⁰ S. Welinski, A. Ferrier, M. Afzelius, and P. Goldner, High-resolution optical spectroscopy and magnetic properties of Yb^{3+} in Y_2SiO_5 , *Phys. Rev. B* **94**, 155116 (2016).
- ³¹ A. Tiranov, A. Ortu, S. Welinski, A. Ferrier, P. Goldner, N. Gisin, and M. Afzelius, Spectroscopic study of hyperfine properties in $^{171}\text{Yb}^{3+}:\text{Y}_2\text{SiO}_5$, *Phys. Rev. B* **98**, 195110 (2018).
- ³² H.-J. Lim, S. Welinski, A. Ferrier, P. Goldner, and J. J. L. Morton, Coherent spin dynamics of ytterbium ions in yttrium orthosilicate, *Phys. Rev. B* **97**, 064409 (2018).
- ³³ J. M. Kindem, J. G. Bartholomew, P. J. T. Woodburn, T. Zhong, I. Craiciu, R. L. Cone, C. W. Thiel, and A. Faraon, Characterization of $^{171}\text{Yb}^{3+}:\text{YVO}_4$ for photonic quantum technologies, *Phys. Rev. B* **98**, 85 (2018).
- ³⁴ P. E. Jessop and A. Szabo, Optical Hole-Burning and Ground State Energy Transfer in Ruby, in *Laser Spectroscopy V* (Springer, Berlin, Heidelberg, Berlin, Heidelberg, 1981) pp. 408–411.
- ³⁵ R. M. Macfarlane and R. M. Shelby, Coherent transient and holeburning spectroscopy of rare earth ions in solids, in *Spectroscopy of Solids Containing Rare Earth Ions*, edited by A. A. Kaplyanskii and R. M. Macfarlane (North-Holland, Amsterdam, 1987) pp. 51–184.
- ³⁶ M. Businger, A. Tiranov, K. T. Kaczmarek, S. Welinski, A. Ferrier, P. Goldner, and M. Afzelius, Optical spin-wave storage in a solid-state hybridized electron-nuclear spin ensemble, *arXiv* (2019), 1907.11571v1 .
- ³⁷ A. M. Stoneham, Shapes of inhomogeneously broadened resonance lines in solids, *Rev. Mod. Phys.* **41**, 82 (1969).
- ³⁸ S. Probst, H. Rotzinger, A. V. Ustinov, and P. A. Bushev, Microwave multimode memory with an erbium spin ensemble, *Phys. Rev. B* **92**, 014421 (2015).
- ³⁹ E. Z. Cruzeiro, A. Tiranov, I. Usmani, C. Laplane, J. Lavoie, A. Ferrier, P. Goldner, N. Gisin, and M. Afzelius, Spectral hole lifetimes and spin population relaxation dynamics in neodymium-doped yttrium orthosilicate, *Phys. Rev. B* **95**, 205119 (2017).
- ⁴⁰ R. W. Equall, Y. Sun, R. L. Cone, and R. M. Macfarlane, Ultraslow optical dephasing in $\text{Eu}^{3+}:\text{Y}_2\text{SiO}_5$, *Phys. Rev. Lett.* **72**, 2179 (1994).
- ⁴¹ B. Casabone, J. Benedikter, T. Hümmer, F. Oehl, K. d. O. Lima, T. W. Hänsch, A. Ferrier, P. Goldner, H. de Riedmatten, and D. Hunger, Cavity-enhanced spectroscopy of a few-ion ensemble in $\text{Eu}^{3+}:\text{Y}_2\text{O}_3$, *New J. Phys.* **20**, 095006 (2018).
- ⁴² L. Veissier, M. Falamarzi, T. Lutz, E. Saglamyurek, C. W. Thiel, R. L. Cone, and W. Tittel, Optical decoherence and spectral diffusion in an erbium-doped silica glass fiber featuring long-lived spin sublevels, *Phys. Rev. B* **94**, 55 (2016).
- ⁴³ M. Afzelius, M. U. Staudt, H. de Riedmatten, N. Gisin, O. Guillot-Noël, P. Goldner, R. Marino, P. Porcher, E. Cavalli, and M. Bettinelli, Efficient optical pumping of Zeeman spin levels in $\text{Nd}^{3+}:\text{YVO}_4$, *J. Lumin.* **130**, 1566 (2010).
- ⁴⁴ S. R. Hastings-Simon, B. Lauritzen, M. U. Staudt, J. L. M. van Mechelen, C. Simon, H. de Riedmatten, M. Afzelius, and N. Gisin, Zeeman-level lifetimes in $\text{Er}^{3+}:\text{Y}_2\text{SiO}_5$, *Phys. Rev. B* **78**, 085410 (2008).
- ⁴⁵ Y. C. Sun, Rare Earth Materials in Optical Storage and Data Processing Applications, in *Spectroscopic properties of rare earths in optical materials*, edited by G. Liu and B. Jacquier (Springer, Berlin, 2005) pp. 379–429.
- ⁴⁶ F. Bussièrès, N. Sangouard, M. Afzelius, H. de Riedmatten, C. Simon, and W. Tittel, Prospective applications of optical quantum memories, *Journal of Modern Optics* **60**, 1519 (2013).
- ⁴⁷ B. Car, L. Veissier, A. Louchet-Chauvet, J.-L. Le Gouët, and T. Chanelière, Optical study of the anisotropic erbium spin flip-flop dynamics, *arXiv* (2018), 1811.10285v1 .
- ⁴⁸ A. Kiel and W. Mims, Paramagnetic Relaxation Measurements on Ce, Nd, and Yb in CaWO_4 by an Electron Spin-Echo Method, *Phys. Rev.* **161**, 386 (1967).

**Coherence enhancement by optically induced electron spin polarization
in a rare-earth doped single crystal - Supplementary information**

VI. OPTICAL PUMPING

A. Populations

Since we are using an isotopically purified sample, the main contribution to the absorption spectra are composed of the 16 different optical transitions belonging to the $S = 1/2, I = 1/2$ $^{171}\text{Yb}^{3+}$ ions. A weak contribution of the $S = 1/2, I = 0$ nuclear spin isotopes ($\approx 6\%$ of all Yb^{3+} ions), is observed at 0 GHz, see Fig. 4a. All spectra were fitted using the expression:

$$\alpha(\nu) = \alpha_0 \sum_{i=1..4, j=1..4} k_{ig} \beta_{ij} g(\nu, \nu_{0,ij}, \Gamma_0) + \alpha_1 g(\nu, \nu_1, \Gamma_1). \quad (5)$$

in which the first term on the right hand side corresponds to $^{171}\text{Yb}^{3+}$ and the second term to $I = 0$ isotopes. In Eq. (5), $\alpha(\nu)$ and $\alpha_{0,1}$ are absorption coefficients, ν the frequency, i (j) ground (excited) state labels and β_{ij} the branching ratio between levels i and j (see Table VIA and³⁶). $g(\nu, \nu_k, \Gamma_k)$ are area-normalized Lorentzian functions with full width at half maximum Γ_k and center frequency ν_k ($\int g(\nu, \nu_k, \Gamma_k) d\nu = 1$). Center frequencies were determined from hole burning experiments³¹ and correspond to the scheme in Fig. 4. The ground state populations k_{ig} verify $0 \leq k_{ig} \leq 4$ and $\sum k_{ig} = 4$. These are normalized to their thermal equilibrium values, which for our working temperatures are $k_{ig,eq} = 1$, to a good approximation.

| | 1 _e ⟩ | 2 _e ⟩ | 3 _e ⟩ | 4 _e ⟩ |
|------------------|------------------|------------------|------------------|------------------|
| 1 _g ⟩ | 0.15 | 0.06 | 0.08 | 0.71 |
| 2 _g ⟩ | 0.06 | 0.19 | 0.71 | 0.04 |
| 3 _g ⟩ | 0.07 | 0.71 | 0.16 | 0.06 |
| 4 _g ⟩ | 0.72 | 0.04 | 0.05 | 0.19 |

TABLE I: Branching ratios for $^{171}\text{Yb}^{3+}:\text{Y}_2\text{SiO}_5$ in site 2 and light polarized along D_2 axis using spectral holeburning technique³⁶.

The absorption spectrum recorded at 2 K without prior optical pumping (OP) was first used to determine $\Gamma_{0,1}$ and $\alpha_{0,1}$. In this case, the $^{171}\text{Yb}^{3+}$ population is equally distributed into the four hyperfine ground states and $k_{ig} = k_{ig,eq} = 1$. Best fit values were $\Gamma_0 = 572 \pm 40$ MHz, $\Gamma_1 = 540 \pm 100$ MHz, $\alpha_0 = 1.37 \pm 0.16$ cm⁻¹ and $\alpha_1 = 0.32 \pm 0.08$ cm⁻¹. Experimental and fitted spectra are shown in Fig. 4b.

Spectra obtained after DEOP were fitted by varying k_{ig} coefficients while keeping $\Gamma_{0,1}$ to the previous values. In some cases, adjustments of α_0 ($\pm 6\%$) and α_1 ($\pm 10\%$) were needed due to small changes in experimental conditions (light polarization, beam alignment with respect to sample). Fig. 5b displays the fit of the spectra in Fig. 1c of the main text resulting in $k_{1g}, k_{2g}, k_{3g}, k_{4g} = 1.67 \pm 0.30, 1.28 \pm 0.36, 1.01 \pm 0.12, 0.04 \pm 0.04$.

VII. DEOP MODELING

A. Qualitative mechanism

The cartoon shown in Fig. 6 explains the mechanism of Diffusion Enhanced Optical Pumping using a simplified system. Here, the ground state is composed of two spin levels and we consider only one optically excited state. Optical pumping (OP) is applied along the transition connecting the higher ground state spin level to the excited state. Ions in the excited state can relax towards the lower spin state, which results in spin polarization. However, since the optical transition is inhomogeneously broaden, the laser is resonant only with a subgroup of all ions. Relaxation of individual spins by interaction with the lattice is assumed to be very slow. At thermal equilibrium, both ground state spin levels are equally populated. DEOP can be described in the following way: an optically pumped spin initially in the higher spin state is transferred to the lower state. This spin can flip-flop with a non-pumped neighbor in the higher spin state. The pumped spin goes back to the higher state, while the neighbor goes to the lower state. If that happens, the pumped spin is transferred again to the lower state, resulting in two spins in the lower state. The neighboring spin can further flip-flop with another non-pumped spin in the higher state, after which the previous sequence can repeat, eventually leading to three spins in the lower state. In this way, the whole system of pumped

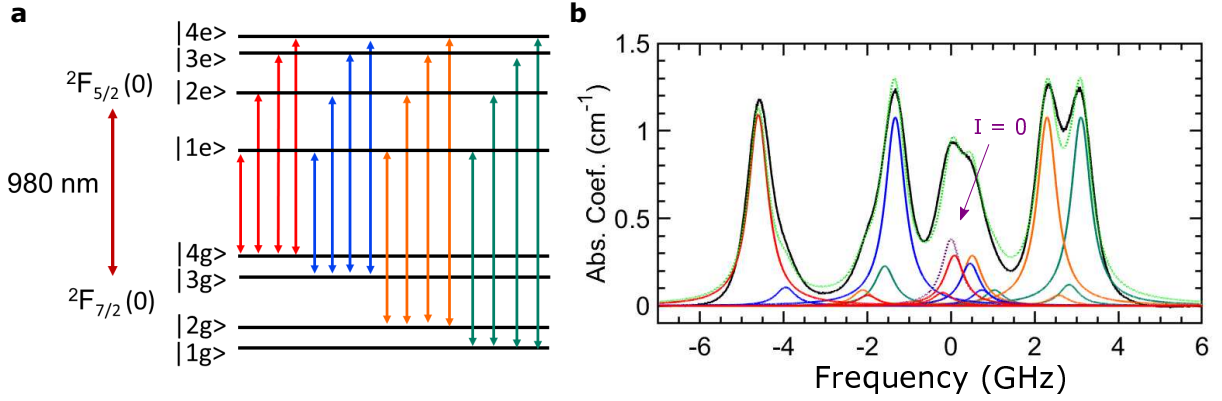


FIG. 4: **a.** Energy diagram of the hyperfine structure of $^{171}\text{Yb}^{3+}$ in Y_2SiO_5 in site 2 for $^2\text{F}_{7/2}(0)$ and $^2\text{F}_{5/2}(0)$. The different colors correspond to the optical transitions connecting the same ground state spin level. **b.** Absorption spectrum at 2 K without prior OP. The different optical transitions constituting the whole absorption spectrum are shown. Their color correspond to the arrow ones in the energy diagram. The residual absorption line from $I = 0$ Yb^{3+} isotopes is observed. The green dashed line represents the fitted curve $\alpha(\nu)$ defined in Eq. (5).

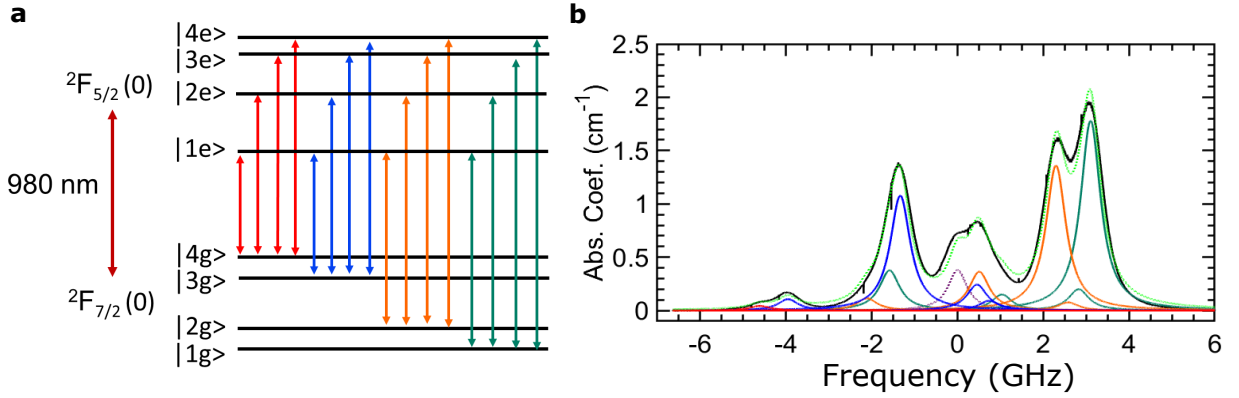


FIG. 5: **a,b** Same as in Fig. 4a,b but with the absorption spectrum recorded after 20 s of OP at -4.8 GHz (Fig. 1c of the main text). The fit gives $k_{1g}, k_{2g}, k_{3g}, k_{4g} = 1.67 \pm 0.30, 1.28 \pm 0.36, 1.01 \pm 0.12, 0.04 \pm 0.04$.

and non-pumped spins can be completely polarized. Qualitatively this requires that the optical pump rate is higher than the flip-flop rate, such that the optically pumped spin spends most of their time in their lower state, while the flip-flop rate should be higher than the spin lattice relaxation rate.

B. Rate equation modeling of DEOP

Here, we use the same energy level scheme as described above for $^{171}\text{Yb}^{3+}$ spins. Therefore, instead of the 4 levels resulting from the low-symmetry anisotropic hyperfine interaction, we consider a $S = 1/2$ spin system. The A-spins are optically pumped and assumed to be non-interacting with each other because of their low concentration. This is justified because the pump laser is much narrower than the optical inhomogeneous broadening. However, they interact with the non-pumped B-spins via magnetic dipole-dipole interactions, see Fig. 7. For A-spins, the optical pumping is resonant with the transition connecting the upper ground state level and the excited state. The effective pumping rate to the lower level is noted R_0 . It takes into account the optical excitation rate R_L from $|+\rangle$ to $|e\rangle$, the excited state radiative population lifetime $T_{1,o}$ and the branching ratio β for $|e\rangle \leftrightarrow |-\rangle$ transition. In our experimental conditions, $R_L \gg 1/T_{1,o}$ and $R_0 = \beta/T_{1,o}$. The population in the upper and lower ground states of A- and B-spins can also relax to each other through spin-lattice relaxation (SLR) at the same rate rate R . Although each A-spin has presumably a different environment in terms of distances and directions of neighboring B-spins, we do not take it into account and consider an average probability $p_A^{+,-}$ for A-spins to be in the upper or lower state.

The B-spins are not pumped, and, since they are in higher concentration, they interact with each other through

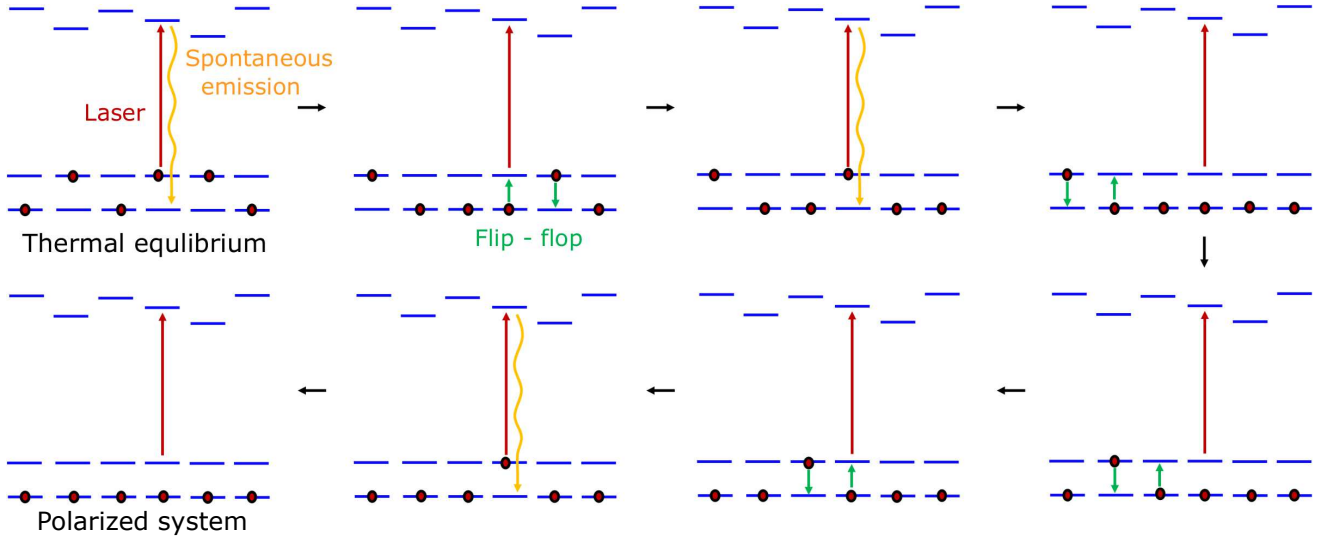


FIG. 6: Qualitative mechanism for DEOP.

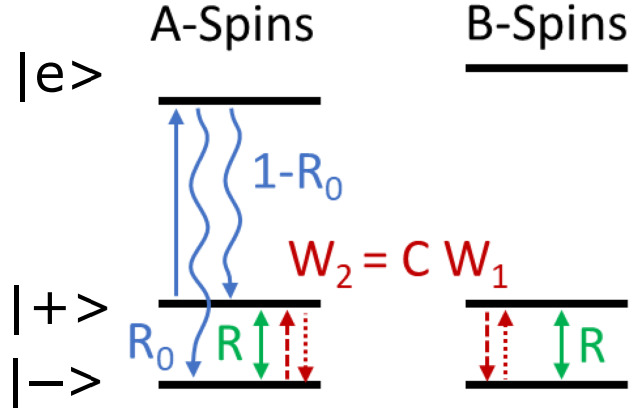


FIG. 7: Spin 1/2 model scheme.

resonant spin flip-flops mediated by the magnetic dipole-dipole interaction. This interaction is assumed to be fast enough on the time scale of the experiment so that all B-spins have the same probability $p_B^{+,-}$ of occupying the upper or lower states. The rate equation for an A-spin i is:

$$\frac{dp_{A,i}^+}{dt} = -(R_0 + R)p_{A,i}^+ + R(1 - p_{A,i}^+) - \sum_{j,B} [W_{ij}p_{A,i}^+(1 - p_{B,j}^+) - W_{ij}(1 - p_{A,i}^+)p_{B,j}^+], \quad (6)$$

where W_{ij} is the flip-flop rate between A-spin i and B-spin j . We used $p_{X,i}^- = 1 - p_{X,i}^+$. According to the above assumptions, subscripts i and j can be dropped for probabilities and $\sum_{j,B} W_{ij}$ does not depend on i . Eq. (6) is then written as:

$$\begin{aligned} \frac{dp_A^+}{dt} &= -(R_0 + R)p_A^+ + R(1 - p_A^+) - \left[\sum_{j,B} W_{ij} \right] [p_A^+(1 - p_B^+) - (1 - p_A^+)p_B^+] \\ &= -(R_0 + R)p_A^+ + R(1 - p_A^+) - W_1 [p_A^+(1 - p_B^+) - (1 - p_A^+)p_B^+] \\ &= -(R_0 + R)p_A^+ + R(1 - p_A^+) - W_1 [p_A^+ - p_B^+]. \end{aligned} \quad (7)$$

Similarly we have for B-spins:

$$\begin{aligned}\frac{dp_B^+}{dt} &= -Rp_B^+ + R(1 - p_B^+) - \left[\sum_{i,A} W_{ij} \right] [p_B^+(1 - p_A^+) - (1 - p_B^+)p_A^+] \\ &= -Rp_B^+ + R(1 - p_B^+) - W_2 [p_B^+(1 - p_A^+) - (1 - p_B^+)p_A^+] \\ &= -Rp_B^+ + R(1 - p_B^+) - W_2 [p_B^+ - p_A^+].\end{aligned}\quad (8)$$

Since W_1 and W_2 are summed respectively on the B- and A-spins, we have $C = W_2/W_1$, where C is the fraction of pumped spins.

The steady state solution of (7) and (8) is obtained by setting the time derivatives on the left hand side to zero:

$$0 = -(R_0 + R)p_A^{+, \infty} + R(1 - p_A^{+, \infty}) - W_1 [p_A^{+, \infty} - p_B^{+, \infty}] \quad (9)$$

$$0 = -Rp_B^{+, \infty} + R(1 - p_B^{+, \infty}) - W_2 [p_B^{+, \infty} - p_A^{+, \infty}], \quad (10)$$

which gives:

$$p_A^{+, \infty} = \frac{R(2R + W_1 + W_2)}{2R(R_0 + W_1) + W_2(R_0 + 2R) + 4R^2} \quad (11)$$

$$p_B^{+, \infty} = \frac{R(R_0 + 2R + W_1 + W_2)}{2R(R_0 + W_1) + W_2(R_0 + 2R) + 4R^2}. \quad (12)$$

We further assume $R_0 \gg R, W_2$ and $W_1 \gg R, W_2$, because in our system the SLR R rate is small, the optical pumping rate R_0 is strong, and only a small fraction of ions is pumped ($C = W_2/W_1 \ll 1$), as discussed in the main text. We introduce $\beta_o = R/(R_0 + R) \approx R/R_0$ and $\beta_{ff} = W_1/(R_0 + W_1)$ and obtain:

$$p_A^{+, \infty} \approx \frac{W_1}{R_0 + W_1} \left(2 + \frac{R_0 W_1}{R(R_0 + W_1)} C \right)^{-1} \quad (13)$$

$$\approx \frac{\beta_{ff}}{2 + C\beta_{ff}/\beta_o} \quad (14)$$

$$p_B^{+, \infty} \approx \left(2 + \frac{R_0 W_1}{R(R_0 + W_1)} C \right)^{-1} \quad (15)$$

$$\approx \frac{1}{2 + C\beta_{ff}/\beta_o}. \quad (16)$$

The rates at which the steady states are reached can also be obtained from the system of equations (7) and (8). Under the assumption $R, W_2 \ll R_0, W_1$, there is a fast component with a rate $R_0 + R$ and a slow one, called the polarization rate in the main text, with a rate:

$$R_P = R(2 + C\beta_{ff}/\beta_o). \quad (17)$$

R_P is the rate that is determined from the experiments of Fig. 2b, main text.

C. Spin flip-flops

For simplicity we assume the Zeeman g - and hyperfine A -tensors are diagonal in the same basis and have anisotropic form $g_x \neq g_y \neq g_z$ and $A_x \neq A_y \neq A_z$. This assumption is well justified for certain solid-state systems (for example $^{171}\text{Yb}^{3+}:\text{Y}_2\text{SiO}_5$ crystal³¹). In this case, at zero magnetic field, the wavefunctions are given only by the hyperfine tensor, which makes all the levels to be non-degenerate:

$$|1\rangle = (|\uparrow\uparrow\rangle - |\downarrow\downarrow\rangle)/\sqrt{2}, \quad |2\rangle = (|\uparrow\uparrow\rangle + |\downarrow\downarrow\rangle)/\sqrt{2},$$

$$|3\rangle = (|\uparrow\downarrow\rangle - |\downarrow\uparrow\rangle)/\sqrt{2}, \quad |4\rangle = (|\uparrow\downarrow\rangle + |\downarrow\uparrow\rangle)/\sqrt{2}.$$

All the spin transitions, in this situation, are connected purely by S_x ($|1\rangle \leftrightarrow |4\rangle$ and $|2\rangle \leftrightarrow |3\rangle$), S_y ($|1\rangle \leftrightarrow |3\rangle$ and $|2\rangle \leftrightarrow |4\rangle$) or S_z ($|1\rangle \leftrightarrow |2\rangle$ and $|3\rangle \leftrightarrow |4\rangle$) spin 1/2 operators. This strongly simplifies the expression for the dipole-dipole interaction H_{dd} that will contain only corresponding operators. In this case the flip-flop rate estimated by Fermi golden rule $|\langle i, f | H_{dd} | f, i \rangle|^2$ will be proportional to the corresponding element of the g -tensor^{39,47}:

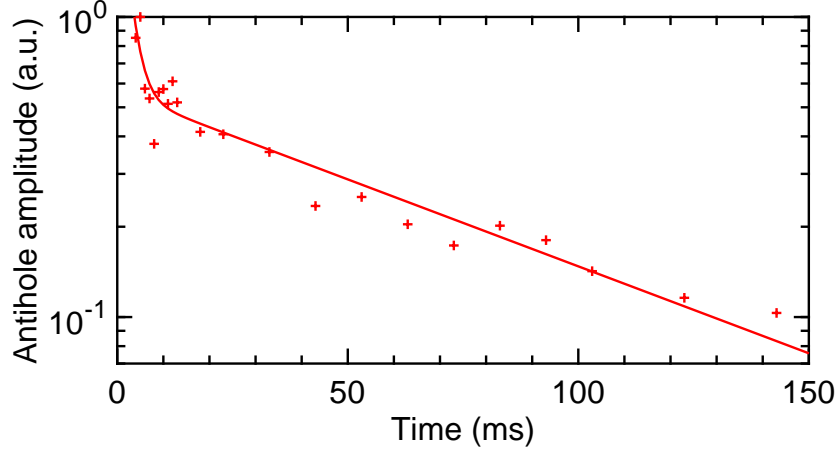


FIG. 8: Decay of an anti-hole in the $|4g\rangle \leftrightarrow |1e\rangle$ line (crosses) and two-exponential fit (solid line).

$$\begin{aligned} \text{for } |1\rangle \leftrightarrow |2\rangle \text{ and } |3\rangle \leftrightarrow |4\rangle: & \propto g_z^4 \\ \text{for } |1\rangle \leftrightarrow |3\rangle \text{ and } |2\rangle \leftrightarrow |4\rangle: & \propto g_y^4, \\ \text{for } |1\rangle \leftrightarrow |4\rangle \text{ and } |2\rangle \leftrightarrow |3\rangle: & \propto g_x^4. \end{aligned}$$

The anisotropy of the g -tensor can lead to dramatically different relaxation times for different transitions. In the case of $^{171}\text{Yb}^{3+}$ in site 2 of Y_2SiO_5 , $g_z = 6.06$, $g_y = 1.5$, $g_x = 0.13$ ³⁰. This predicts a few orders of magnitude variation for different transitions, flip-flops within the $|1\rangle \leftrightarrow |2\rangle$ and $|3\rangle \leftrightarrow |4\rangle$ pairs of levels being much faster than all the other ones.

D. SLR modeling

The recovery time R_c of the $|4g\rangle \leftrightarrow |1e\rangle$ optical line after the OP has been stopped corresponds to spin lattice relaxations. Indeed spin flip-flops do not change overall populations in the case of no optical pumping. R_c has been measured for different temperatures and its variations are shown on Fig 2d in the main text. Those variations can be modeled by considering the one-phonon direct process and two-phonons processes⁴⁸:

$$R_c = \alpha_D \coth\left(\frac{h\nu_{eff}}{2k_B T}\right) + \alpha_R \int_0^{\frac{\pi}{2}} \frac{q^8 e^{-\frac{\theta_D}{T} \sin q} dq}{(1 - e^{-\frac{\theta_D}{T} \sin q})^2 (\theta_E^2 - \theta_D^2 \sin^2 q)^2} \quad (18)$$

In this equation, the same parameters than in a previous study³², $\theta_D = 100$ K and $\theta_E = 337$ K, have been used for the two-phonon part. The direct process term uses the average splitting between $|4g\rangle$ and the three other ground state spin levels, $\nu_{eff} = 2.06$ GHz. The fitted coefficients are $\alpha_D = 3.9 \times 10^{-4} \text{ s}^{-1}$ and $\alpha_R = 0.9 \times 10^{18} \text{ s}^{-1} \cdot \text{K}^4$. The latter value is reasonably close to the one determined in³².

E. Narrow hole decays

In order to compare the W_1 value extracted from the fit in Fig. 2c (main text) to experimental flip-flop rates, we investigated the dynamics of a narrow anti-hole in the $|4g\rangle \leftrightarrow |1e\rangle$ transition. It was obtained by burning a hole close to the center of the $|2g\rangle \leftrightarrow |4e\rangle$ transition at +2.5 GHz (see Fig. 1c, main text) for 10 ms, a duration short enough to avoid DEOP. The anti-hole height was measured at varying delays after the hole burning. Each measurement was preceded by an initialization sequence of 50 pulses scanned over 10 GHz to prevent accumulating populations. Fig. 8 shows the experimental data together with a two-exponential fit, giving rates of 500 and 13 s^{-1} . The larger rate is attributed to the fast $|4g\rangle \leftrightarrow |3g\rangle$ flip-flops and the other one, which correspond to W_1 in the rate equation model, to the intermediate $|4g\rangle \leftrightarrow |2g\rangle$ flip-flops.

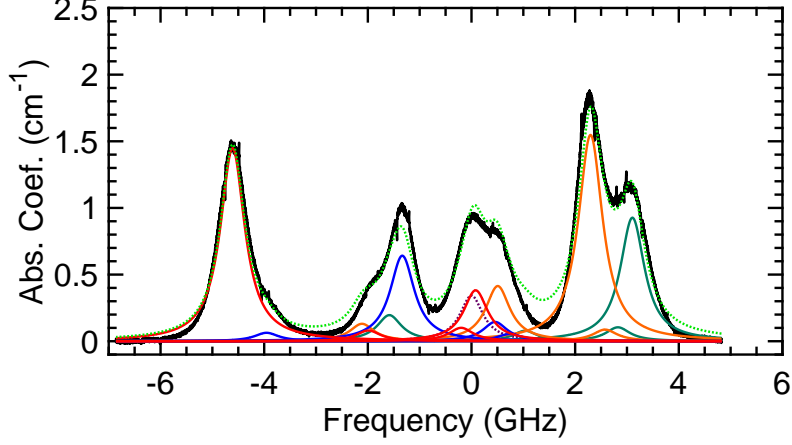


FIG. 9: Same as in Fig. 4a,b but with the absorption spectrum recorded after 0.5 s OP at -1.44 GHz.

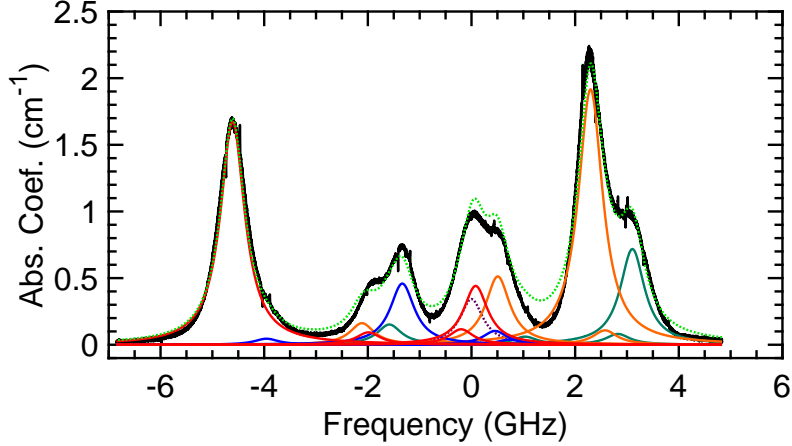


FIG. 10: Same as Fig. 9, but after 1 s OP at -1.44 GHz.

VIII. OPTICAL COHERENCE

A. Populations

For echo measurements under DEOP (Fig. 3, main text), normalized populations ($k_{1g}, k_{2g}, k_{3g}, k_{4g}$) were determined from absorption spectra, as described in section VIA. The spectra and fits are shown in figures 9 to 15, and the corresponding k_{ig} values presented in Table II.

| OP condition | Absorption spectrum | k_1 | k_2 | k_3 | k_4 |
|-----------------------------|---------------------|--------------------|--------------------|--------------------|--------------------|
| No prior OP | Figure 4 | 1 | 1 | 1 | 1 |
| 0.5 s OP laser at -1.44 GHz | Figure 9 | 0.82 ± 0.06 | 1.36 ± 0.08 | 0.56 ± 0.08 | 1.26 ± 0.06 |
| 1 s OP laser at -1.44 GHz | Figure 10 | 0.61 ± 0.06 | 1.62 ± 0.08 | 0.39 ± 0.06 | 1.39 ± 0.06 |
| 2 s OP laser at -1.44 GHz | Figure 11 | 0.27 ± 0.04 | 2.01 ± 0.08 | 0.13 ± 0.12 | 1.59 ± 0.06 |
| 5 s OP laser at -1.44 GHz | Figure 12 | 0.06 ± 0.04 | 2.24 ± 0.08 | 0.05 ± 0.05 | 1.70 ± 0.08 |
| 10 s OP laser at -1.44 GHz | Figure 13 | 0.02 ± 0.02 | 2.30 ± 0.12 | 0.02 ± 0.02 | 1.70 ± 0.06 |
| 1 s OP laser at +2.67 GHz | Figure 14 | 0.50 ± 0.02 | 0.10 ± 0.02 | 1.64 ± 0.08 | 1.76 ± 0.04 |
| 10 s OP laser at +2.67 GHz | Figure 15 | 0.02 ± 0.02 | 0.02 ± 0.02 | 1.95 ± 0.10 | 2.05 ± 0.08 |

TABLE II: Normalized ground state populations corresponding to the different OP conditions.

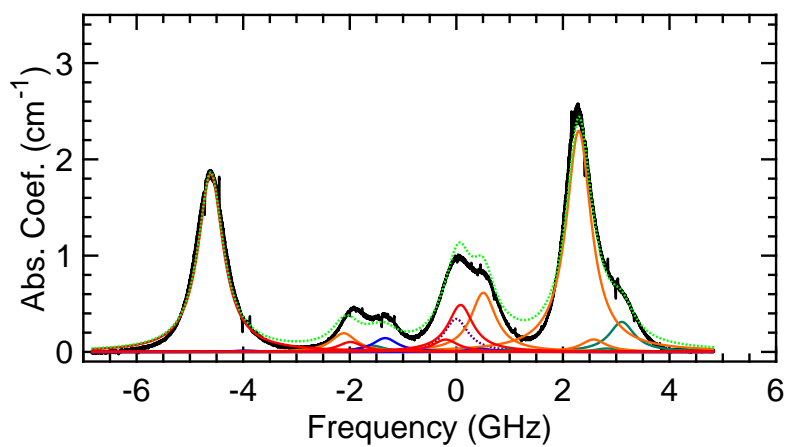


FIG. 11: Same as Fig. 9, but after 2 s OP at -1.44 GHz.

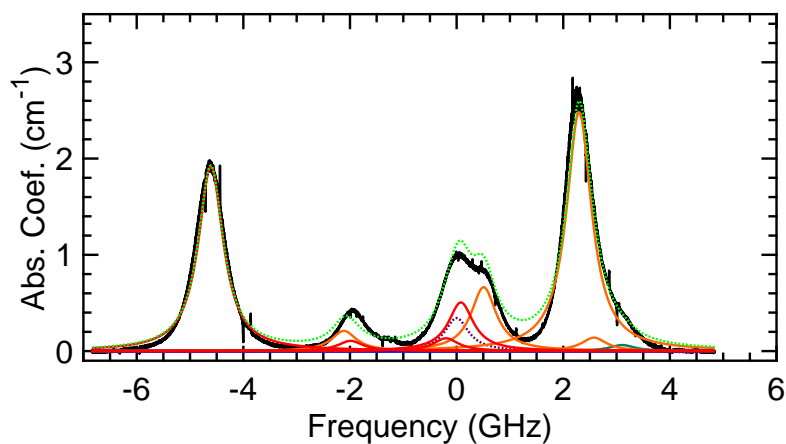


FIG. 12: Same as Fig. 9, but after 5 s OP at -1.44 GHz.

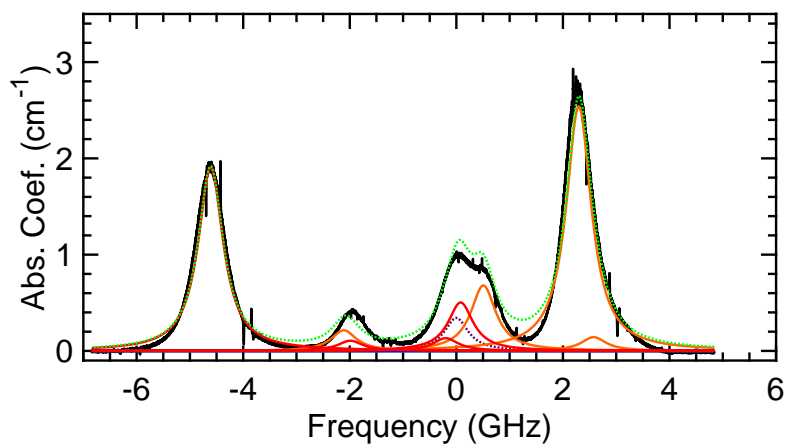


FIG. 13: Same as Fig. 9, but after 10 s OP at -1.44 GHz.

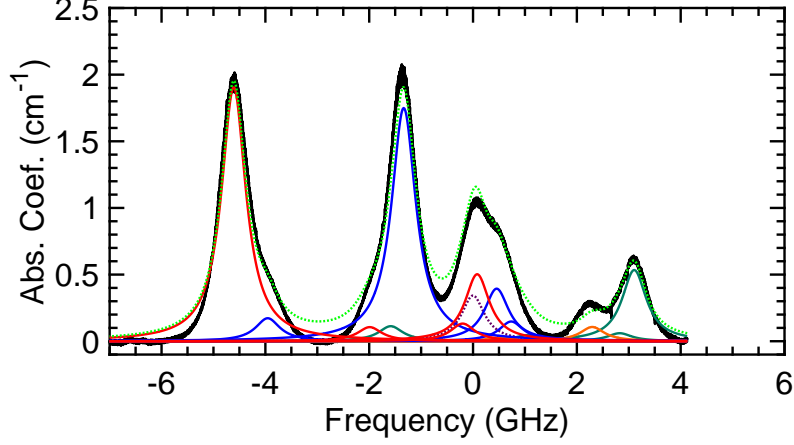


FIG. 14: Same as Fig. 9, but after 1 s OP at +2.67 GHz.

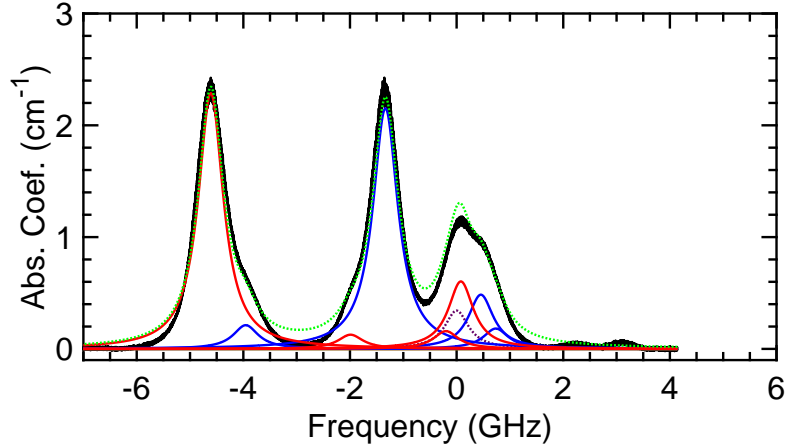


FIG. 15: Same as Fig. 9, but after 10 s OP at +2.67 GHz.

B. Spin coherence

We performed another set of measurements to investigate the effect of the optical pumping on the spin coherence at 3 K. For this, we measured the spin coherence time $T_{2,s}$ through optical detection of a spin echo in a Hahn sequence using Raman heterodyne scattering (RHS), see¹⁷. All spin echo measurements were carried out on the $|4g\rangle \leftrightarrow |3g\rangle$ transition (655 MHz) of site 2 by varying total population in $|3g\rangle$ and $|4g\rangle$ states for different optical pumping conditions.

In a first set of measurements, the optical pumping was performed with the laser set between $|4g\rangle \leftrightarrow |1e\rangle$ and $|3g\rangle \leftrightarrow |1e\rangle$ optical transitions to polarize the spin ensemble into $|1g\rangle$ and $|2g\rangle$ spin states. The optical pumping, in this set of measurements, is done by scanning the laser over the inhomogeneous broadening during 500 ms to speed up the pumping process and polarize larger spin population. The second laser was used to detect the spin echo signal through RHS detection and was set to $|4g\rangle \leftrightarrow |1e\rangle$ transition. The populations in each state were estimated using separate optical absorption measurements utilizing the previously measured optical branching ratio table (see section VIA). As a result, we observe a substantial increase of the spin coherence time up to 2.5 ms for the strongest polarization of the spin ensemble (Fig. 16). We note that similar values were measured previously in this sample¹⁷.

On a second stage, the optical pumping was performed with a laser set between the $|1g\rangle \leftrightarrow |4e\rangle$ and the $|2g\rangle \leftrightarrow |3e\rangle$ optical transitions to inverse the polarization and have higher population of $|3g\rangle$ and $|4g\rangle$ spin states. Additionally the transition $|3g\rangle \leftrightarrow |2e\rangle$ was weakly driven to initialize the spin ensemble to create initial spin polarization for the RHS generation. As a result, a reduction of the spin coherence time up to 0.2 ms was measured (Fig. 16).

We attribute this behavior to the modification of the spin flip-flop process on $|3g\rangle \leftrightarrow |4g\rangle$ transition, directly limiting

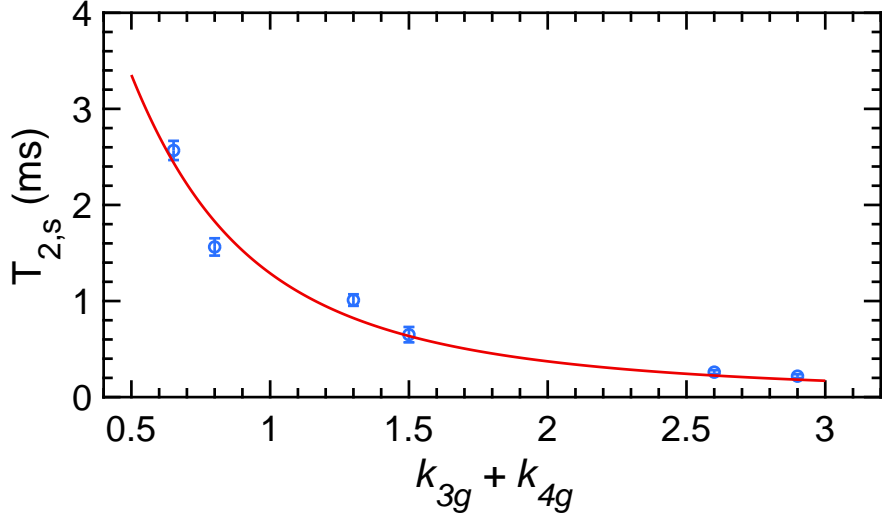


FIG. 16: Spin coherence times $T_{2,s}$ of $|4g\rangle \leftrightarrow |3g\rangle$ transition for various initial populations in $|3g\rangle$ and $|4g\rangle$ spin states (circles) and fit to a model of coherence limited by population lifetimes (red line, see text).

the spin coherence time through $|3g\rangle$ and $|4g\rangle$ population lifetimes. Indeed, in contrast to the optical coherence study, the increase of the spin coherence was measured when pumping into both $|3g\rangle$ and $|4g\rangle$. In this case, the optical pumping reduces the flip-flop rate on $|3g\rangle \leftrightarrow |4g\rangle$ transition, by proportionally increasing the cross relaxation between $|1g\rangle \leftrightarrow |2g\rangle$ ground states. Assuming that the flip-flop probabilities on $|1g\rangle \leftrightarrow |2g\rangle$ and $|3g\rangle \leftrightarrow |4g\rangle$ transition are the same, such population distribution doesn't lead to an overall reduction of the magnetic field noise created by the flip-flops, which could potentially explain the coherence increase. In this situation, the increase of the spin coherence on $|3g\rangle \leftrightarrow |4g\rangle$ transition can be explained by the increase of $|3g\rangle$ and $|4g\rangle$ population lifetimes induced by the reduction of flip-flops between $|3g\rangle$ and $|4g\rangle$ spin states.

To estimate the spin flip-flop rate we apply the simple coherence time model from the main text (Eq. (3)). For this we assume that the pure dephasing term is constant for different pumping conditions and the lifetime of the ground states is limited by the flip-flop process on $|4g\rangle \leftrightarrow |3g\rangle$ transition. The last assumption results in quadratic dependence on the population in these two spin states:

$$T_{2,s}^{-1} = R_{ff} k'_{3g} k'_{4g} + \pi \Gamma_{\phi}, \quad (19)$$

where k'_{3g} and k'_{4g} are the populations after applying the $\pi/2$ microwave pulse for the spin echo measurement. Since the first $\pi/2$ microwave pulse will average initial populations between $|3g\rangle$ and $|4g\rangle$ spin states we can write $k'_{3g} k'_{4g} = ((k_{3g} + k_{4g})/2)^2$. Initial populations k_{3g} , k_{4g} for various optical pumping conditions were measured by fitting the absorption profile taken before applying the microwave sequence. By fitting the measured coherence times $T_{2,s}$ (Fig. 16) using Eq. (19) we estimate the flip-flop rate to be 0.39 ms for equal population of all spin states, with spin coherence time limit of $(\pi \Gamma_{\phi})^{-1} = 7.2$ ms.

The estimated equilibrium flip-flop process will limit the optical coherence to 0.8 ms which is more than two times bigger than the optical coherence time of 0.3 ms measured without optical pumping. This can be explained by a stronger sensitivity of the optical transition frequency to magnetic field fluctuations coming from the crystalline spin bath, which are modified by the optical pumping.

IX. DISCUSSION

A. Polarization into a single hyperfine level

Here the laser is set at +0.22 GHz on the absorption spectrum shown on Fig. 17. At this frequency, the laser is resonant with some ions in $|2g\rangle$, $|3g\rangle$ and $|4g\rangle$, through the optical transitions $|2g\rangle \leftrightarrow |2e\rangle$, $|3g\rangle \leftrightarrow |3e\rangle$, $|3g\rangle \leftrightarrow |4e\rangle$, $|4g\rangle \leftrightarrow |3e\rangle$ and $|4g\rangle \leftrightarrow |4e\rangle$ (see Fig. 4b). After 20s of OP duration, the absorption spectrum shown in Fig. 17 is obtained. Corresponding normalized populations are $k_1 = 3.84 \pm 0.02$, $k_2 = 0.04 \pm 0.02$, $k_3 = 0.12 \pm 0.12$, $k_4 = 0.12 \pm 0.04$, which means that 96 ± 1 % of the total population in the volume addressed by the laser has been

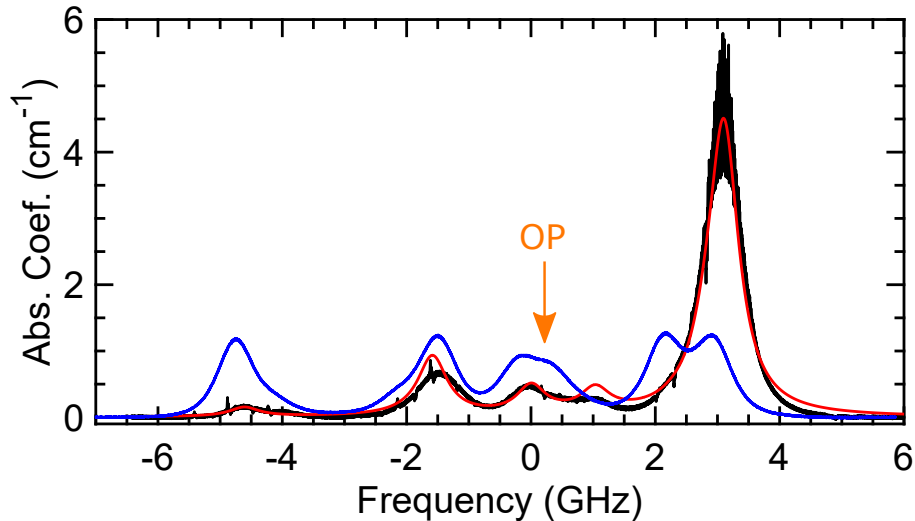


FIG. 17: Absorption spectrum after 20 s OP for the laser set at +0.22 GHz (black line) and fit (red line). Corresponding normalized populations are: $k_1 = 3.84 \pm 0.02$, $k_2 = 0.04 \pm 0.02$, $k_3 = 0.12 \pm 0.12$, $k_4 = 0.12 \pm 0.04$. Blue line: absorption spectrum at thermal equilibrium.

stored into the $|1_g\rangle$ state. As expected, we can see that the $|1_g\rangle \leftrightarrow |4_e\rangle$ absorption has reached a value almost four times larger than at thermal equilibrium.

-
- * Present affiliation : Department of Electrical Engineering, Princeton University, Princeton, NJ 08544, USA
† Present affiliation : The Niels Bohr Institute, University of Copenhagen, DK-2100 Copenhagen Ø, Denmark
‡ philippe.goldner@chimieparistech.psl.eu
- ¹ M. Atatüre, D. Englund, N. Vamivakas, S.-Y. Lee, and J. Wrachtrup, Material platforms for spin-based photonic quantum technologies, *Nat. Rev. Mater.* **3**, 1 (2018).
 - ² F. Bussi eres, C. Clausen, A. Tiranov, B. Korzh, V. B. Verma, S. W. Nam, F. Marsili, A. Ferrier, P. Goldner, H. Herrmann, C. Silberhorn, W. Sohler, M. Afzelius, and N. Gisin, Quantum teleportation from a telecom-wavelength photon to a solid-state quantum memory, *Nat. Photonics* **8**, 775 (2014).
 - ³ B. Hensen, H. Bernien, A. E. Dr eau, A. Reiserer, N. Kalb, M. S. Blok, J. Ruitenber, R. F. L. Vermeulen, R. N. Schouten, C. Abell an, W. Amaya, V. Pruneri, M. W. Mitchell, M. Markham, D. J. Twitchen, D. Elkouss, S. Wehner, T. H. Taminiau, and R. Hanson, Loophole-free Bell inequality violation using electron spins separated by 1.3 kilometres, *Nature* **526**, 682 (2015).
 - ⁴ H. J. Kimble, The quantum internet, *Nature* **453**, 1023 (2008).
 - ⁵ J. M. Boss, K. S. Cujia, J. Zopes, and C. L. Degen, Quantum sensing with arbitrary frequency resolution, *Science* **356**, 837 (2017).
 - ⁶ M. Zhong, M. P. Hedges, R. L. Ahlefeldt, J. G. Bartholomew, S. E. Beavan, S. M. Wittig, J. J. Longdell, and M. J. Sellars, Optically addressable nuclear spins in a solid with a six-hour coherence time, *Nature* **517**, 177 (2015).
 - ⁷ D. Serrano, J. Karlsson, A. Fossati, A. Ferrier, and P. Goldner, All-optical control of long-lived nuclear spins in rare-earth doped nanoparticles, *Nat. Commun.* **9**, 2127 (2018).
 - ⁸ T. B ottger, C. W. Thiel, Y. Sun, and R. L. Cone, Optical decoherence and spectral diffusion at $1.5\mu\text{m}$ in $\text{Er}^{3+}:\text{Y}_2\text{SiO}_5$ versus magnetic field, temperature, and Er^{3+} concentration, *Phys. Rev. B* **73**, 075101 (2006).
 - ⁹ H. S. Knowles, D. M. Kara, and M. Atat ure, Observing bulk diamond spin coherence in high-purity nanodiamonds, *Nat. Mater.* **13**, 21 (2014).
 - ¹⁰ G. Balasubramanian, P. Neumann, D. Twitchen, M. Markham, R. Kolesov, N. Mizuochi, J. Isoya, J. Achard, J. Beck, J. Tissler, V. Jacques, P. R. Hemmer, F. Jelezko, and J. Wrachtrup, Ultralong spin coherence time in isotopically engineered diamond, *Nat. Mater.* **8**, 383 (2009).
 - ¹¹ A. M. Tyryshkin, S. Tojo, J. J. L. Morton, H. Riemann, N. V. Abrosimov, P. Becker, H.-J. Pohl, T. Schenkel, M. L. W. Thewalt, K. M. Itoh, and S. A. Lyon, Electron spin coherence exceeding seconds in high-purity silicon, *Nat. Mater.* **11**, 143 (2011).
 - ¹² T. B ottger, C. W. Thiel, R. L. Cone, and Y. Sun, Effects of magnetic field orientation on optical decoherence in $\text{Er}^{3+}:\text{Y}_2\text{SiO}_5$, *Phys. Rev. B* **79**, 115104 (2009).

- ¹³ M. Rancic, M. P. Hedges, R. L. Ahlefeldt, and M. J. Sellars, Coherence time of over a second in a telecom-compatible quantum memory storage material, *Nat. Phys.* **14**, 50 (2017).
- ¹⁴ N. Kukharchyk, D. Sholokhov, O. Morozov, S. L. Korableva, A. A. Kalachev, and P. A. Bushev, Optical coherence of $^{166}\text{Er}:\text{LiYF}_4$ crystal below 1 K, *New J. Phys.* **20**, 023044 (2018).
- ¹⁵ E. Fraval, M. J. Sellars, and J. J. Longdell, Method of Extending Hyperfine Coherence Times in $\text{Pr}^{3+}\text{Y}_2\text{SiO}_5$, *Phys. Rev. Lett.* **92**, 077601 (2004).
- ¹⁶ G. Wolfowicz, A. M. Tyryshkin, R. E. George, H. Riemann, N. V. Abrosimov, P. Becker, H.-J. Pohl, M. L. W. Thewalt, S. A. Lyon, and J. J. L. Morton, Atomic clock transitions in silicon-based spin qubits, *Nat. Nanotechnol.* **8**, 561 (2013).
- ¹⁷ A. Ortu, A. Tiranov, S. Welinski, F. Fröwis, N. Gisin, A. Ferrier, P. Goldner, and M. Afzelius, Simultaneous coherence enhancement of optical and microwave transitions in solid-state electronic spins, *Nat. Mater.* **17**, 671 (2018).
- ¹⁸ L. Viola and S. Lloyd, Dynamical suppression of decoherence in two-state quantum systems, *Phys. Rev. A* **58**, 2733 (1998).
- ¹⁹ M. Lovrić, D. Suter, A. Ferrier, and P. Goldner, Faithful Solid State Optical Memory with Dynamically Decoupled Spin Wave Storage, *Phys. Rev. Lett.* **111**, 020503 (2013).
- ²⁰ P. Goldner, A. Ferrier, and O. Guillot-Noël, Rare Earth-Doped Crystals for Quantum Information Processing, in *Handbook on the Physics and Chemistry of Rare Earths*, edited by J.-C. G. Bünzli and V. K. Pecharsky (Elsevier, Amsterdam, 2015) pp. 1–78.
- ²¹ E. Saglamyurek, N. Sinclair, J. Jin, J. A. Slater, D. Oblak, F. Bussièeres, M. George, R. Ricken, W. Sohler, and W. Tittel, Broadband waveguide quantum memory for entangled photons, *Nature* **469**, 512 (2011).
- ²² Z.-Q. Zhou, W.-B. Lin, M. Yang, C.-F. Li, and G.-C. Guo, Realization of Reliable Solid-State Quantum Memory for Photonic Polarization Qubit, *Phys. Rev. Lett.* **108**, 190505 (2012).
- ²³ T. Zhong, J. M. Kindem, J. G. Bartholomew, J. Rochman, I. Craiciu, E. Miyazono, M. Bettinelli, E. Cavalli, V. Verma, S. W. Nam, F. Marsili, M. D. Shaw, A. D. Beyer, and A. Faraon, Nanophotonic rare-earth quantum memory with optically controlled retrieval, *Science* **357**, 1392 (2017).
- ²⁴ C. Laplane, P. Jobez, J. Etesse, N. Gisin, and M. Afzelius, Multimode and Long-Lived Quantum Correlations Between Photons and Spins in a Crystal, *Phys. Rev. Lett.* **118**, 210501 (2017).
- ²⁵ A. Walther, L. Rippe, Y. Yan, J. Karlsson, D. Serrano, A. N. Nilsson, S. Bengtsson, and S. Kröll, High-fidelity readout scheme for rare-earth solid-state quantum computing, *Phys. Rev. A* **92**, 022319 (2015).
- ²⁶ A. M. Dibos, M. Raha, C. M. Phenicie, and J. D. Thompson, Atomic Source of Single Photons in the Telecom Band, *Phys. Rev. Lett.* **120**, 243601 (2018).
- ²⁷ T. Zhong, J. M. Kindem, J. G. Bartholomew, J. Rochman, I. Craiciu, V. Verma, S. W. Nam, F. Marsili, M. D. Shaw, A. D. Beyer, and A. Faraon, Optically Addressing Single Rare-Earth Ions in a Nanophotonic Cavity, *Phys. Rev. Lett.* **121**, 183603 (2018).
- ²⁸ L. A. Williamson, Y.-H. Chen, and J. J. Longdell, Magneto-Optic Modulator with Unit Quantum Efficiency, *Phys. Rev. Lett.* **113**, 203601 (2014).
- ²⁹ S. Welinski, P. J. T. Woodburn, N. Lauk, R. L. Cone, C. Simon, P. Goldner, and C. W. Thiel, Electron Spin Coherence in Optically Excited States of Rare-Earth Ions for Microwave to Optical Quantum Transducers, *Phys. Rev. Lett.* **122**, 247401 (2019).
- ³⁰ S. Welinski, A. Ferrier, M. Afzelius, and P. Goldner, High-resolution optical spectroscopy and magnetic properties of Yb^{3+} in Y_2SiO_5 , *Phys. Rev. B* **94**, 155116 (2016).
- ³¹ A. Tiranov, A. Ortu, S. Welinski, A. Ferrier, P. Goldner, N. Gisin, and M. Afzelius, Spectroscopic study of hyperfine properties in $^{171}\text{Yb}^{3+}:\text{Y}_2\text{SiO}_5$, *Phys. Rev. B* **98**, 195110 (2018).
- ³² H.-J. Lim, S. Welinski, A. Ferrier, P. Goldner, and J. J. L. Morton, Coherent spin dynamics of ytterbium ions in yttrium orthosilicate, *Phys. Rev. B* **97**, 064409 (2018).
- ³³ J. M. Kindem, J. G. Bartholomew, P. J. T. Woodburn, T. Zhong, I. Craiciu, R. L. Cone, C. W. Thiel, and A. Faraon, Characterization of $^{171}\text{Yb}^{3+}:\text{YVO}_4$ for photonic quantum technologies, *Phys. Rev. B* **98**, 85 (2018).
- ³⁴ P. E. Jessop and A. Szabo, Optical Hole-Burning and Ground State Energy Transfer in Ruby, in *Laser Spectroscopy V* (Springer, Berlin, Heidelberg, Berlin, Heidelberg, 1981) pp. 408–411.
- ³⁵ R. M. Macfarlane and R. M. Shelby, Coherent transient and holeburning spectroscopy of rare earth ions in solids, in *Spectroscopy of Solids Containing Rare Earth Ions*, edited by A. A. Kaplyanskii and R. M. Macfarlane (North-Holland, Amsterdam, 1987) pp. 51–184.
- ³⁶ M. Businger, A. Tiranov, K. T. Kaczmarek, S. Welinski, A. Ferrier, P. Goldner, and M. Afzelius, Optical spin-wave storage in a solid-state hybridized electron-nuclear spin ensemble, *arXiv* (2019), 1907.11571v1.
- ³⁷ A. M. Stoneham, Shapes of inhomogeneously broadened resonance lines in solids, *Rev. Mod. Phys.* **41**, 82 (1969).
- ³⁸ S. Probst, H. Rotzinger, A. V. Ustinov, and P. A. Bushev, Microwave multimode memory with an erbium spin ensemble, *Phys. Rev. B* **92**, 014421 (2015).
- ³⁹ E. Z. Cruzeiro, A. Tiranov, I. Usmani, C. Laplane, J. Lavoie, A. Ferrier, P. Goldner, N. Gisin, and M. Afzelius, Spectral hole lifetimes and spin population relaxation dynamics in neodymium-doped yttrium orthosilicate, *Phys. Rev. B* **95**, 205119 (2017).
- ⁴⁰ R. W. Equall, Y. Sun, R. L. Cone, and R. M. Macfarlane, Ultraslow optical dephasing in $\text{Eu}^{3+}:\text{Y}_2\text{SiO}_5$, *Phys. Rev. Lett.* **72**, 2179 (1994).
- ⁴¹ B. Casabone, J. Benedikter, T. Hümmer, F. Oehl, K. d. O. Lima, T. W. Hänsch, A. Ferrier, P. Goldner, H. de Riedmatten, and D. Hunger, Cavity-enhanced spectroscopy of a few-ion ensemble in $\text{Eu}^{3+}:\text{Y}_2\text{O}_3$, *New J. Phys.* **20**, 095006 (2018).
- ⁴² L. Veissier, M. Falamarzi, T. Lutz, E. Saglamyurek, C. W. Thiel, R. L. Cone, and W. Tittel, Optical decoherence and spectral diffusion in an erbium-doped silica glass fiber featuring long-lived spin sublevels, *Phys. Rev. B* **94**, 55 (2016).

- ⁴³ M. Afzelius, M. U. Staudt, H. de Riedmatten, N. Gisin, O. Guillot-Noël, P. Goldner, R. Marino, P. Porcher, E. Cavalli, and M. Bettinelli, Efficient optical pumping of Zeeman spin levels in Nd^{3+} : YVO_4 , *J. Lumin.* **130**, 1566 (2010).
- ⁴⁴ S. R. Hastings-Simon, B. Lauritzen, M. U. Staudt, J. L. M. van Mechelen, C. Simon, H. de Riedmatten, M. Afzelius, and N. Gisin, Zeeman-level lifetimes in Er^{3+} : Y_2SiO_5 , *Phys. Rev. B* **78**, 085410 (2008).
- ⁴⁵ Y. C. Sun, Rare Earth Materials in Optical Storage and Data Processing Applications, in *Spectroscopic properties of rare earths in optical materials*, edited by G. Liu and B. Jacquier (Springer, Berlin, 2005) pp. 379–429.
- ⁴⁶ F. Bussi eres, N. Sangouard, M. Afzelius, H. de Riedmatten, C. Simon, and W. Tittel, Prospective applications of optical quantum memories, *Journal of Modern Optics* **60**, 1519 (2013).
- ⁴⁷ B. Car, L. Veissier, A. Louchet-Chauvet, J.-L. Le Gou et, and T. Chaneli ere, Optical study of the anisotropic erbium spin flip-flop dynamics, *arXiv* (2018), 1811.10285v1 .
- ⁴⁸ A. Kiel and W. Mims, Paramagnetic Relaxation Measurements on Ce, Nd, and Yb in CaWO_4 by an Electron Spin-Echo Method, *Phys. Rev.* **161**, 386 (1967).